Precambrian Research 220–221 (2012) 192–216

Contents lists available at SciVerse ScienceDirect

Precambrian Research

journal homepage: www.elsevier.com/locate/precamres

Diversity of Rhyacian granitoids in the basement of the Neoproterozoic-Early Cambrian Gurupi Belt, northern Brazil: Geochemistry, U–Pb zircon geochronology, and Nd isotope constraints on the Paleoproterozoic magmatic and crustal evolution

Evandro L. Klein[a,*], Joseneusa B. Rodrigues[b], Elem C.S. Lopes[a], Gilvana L. Soledade[a,c,1]

[a] CPRM-Geological Survey of Brazil, Av. Dr. Freitas, 3645, CEP: 66095-110 Belém, PA, Brazil
[b] CPRM-Geological Survey of Brazil, Av. SGAN Q603, conj. J. parte A, CEP: 70830-030 Brasília, DF, Brazil
[c] Universidade Federal do Pará, Programa de Pós-Graduação em Geologia e Geoquímica, CP 1611, CEP: 66075-900 Belém, PA, Brazil

ARTICLE INFO

Article history:
Received 3 May 2012
Received in revised form 28 July 2012
Accepted 14 August 2012
Available online xxx

Keywords:
Paleoproterozoic
Neoproterozoic
Gurupi Belt
U–Pb
Granitoid magmatism
Collision

ABSTRACT

The Gurupi Belt, in northern Brazil, is a Neoproterozoic-Early Cambrian orogen developed at the south-southwestern margin of the São Luís-West African Craton. Several plutonic bodies are exposed as basement units of the Gurupi Belt and represent a variety of granitoid types emplaced at different ages and all show zircon inheritance and chemical and isotopic features that imply participation of reworked Archean to Paleoproterozoic crust in the magma genesis in clear contrast with the juvenile characteristics of the predominant magmatic unit of the neighboring São Luís cratonic fragment, the Tromaí Intrusive Suite of 2167–2147 Ma. The weakly peraluminous, high-K, calc-alkaline biotite-bearing Cantão Granodiorite of 2163 ± 4 Ma has T_{DM} model ages of 2.21–2.92 Ga and εNd values of +2.7 to −7.1. The 2142 ± 9 Ma-old, weakly peraluminous, biotite- and muscovite-bearing Jonasa Granodiorite underwent metamorphism and deformation at 525 Ma and shows T_{DM} model ages of 2.14–2.40 Ga, with εNd values of +3.9 to −0.2. Both are, probably, related to a continental arc setting. A relatively large event of strongly peraluminous granitic magmatism took place between 2116 and 2079 Ma, and comprises the crust-derived, biotite- and muscovite-bearing granites and leucogranites of probable collisional setting belonging to the Japiim, Tamancuoca, Moça and Maria Suprema units. Despite broadly similar, these units show some chemical differences that are interpreted to result from mixtures of variable amounts of sedimentary and igneous sources of Archean to Paleoproterozoic ages. These granites show T_{DM} model ages of 2.19–2.62 Ga and the εNd values range from +3.9 to −0.2, and probably represent collision rocks. Associated in space and time with part of the strongly peraluminous granites, the 2100 ± 21 Ma-old, metaluminous to slightly peralkaline granites, quartz-monzonites and quartz-syenites of the Anelis Intrusive Suite have characteristics of potassic to shoshonitic post-collisional rocks. The suite shows T_{DM} model ages of 2.27–2.48 Ga and εNd values of +0.1 to −2.6. The last known event is represented by the post-orogenic, 2085 ± 4 Ma-old, weakly peraluminous, high-K, calc-alkaline, biotite-bearing Timbozal Monzogranite, with T_{DM} model ages of 2.27–2.58 Ga and εNd values of +1.1 to −2.8.

The strongly peraluminous and different generations of potassic granitoids represent magmatic events with characteristics that may be related to both continental arc subduction and collision processes and indicate that the granitoid bodies represent disrupted fragments of a Rhyacian orogenic belt (continental arc and collision belt) that remains today as basement inliers within the Gurupi Belt in the margin of the São Luís-West African Craton. These sequences, together with the juvenile rocks of the São Luís cratonic fragment, are part of a protracted Rhyacian orogen that evolved from ~2240 Ma to ~2050 Ma, involving accretionary and collision processes. These sequences also correlate in time and several aspects of evolutionary processes with Eburnean-Birimian terranes of the West-African Craton and Trans-Amazonian belts of the Amazonian Craton.

* Corresponding author.
E-mail address: evandro.klein@cprm.gov.br (E.L. Klein).
[1] Present address: Vale S/A, Av. Getulio Vargas, 671, 11° andar, Edificio Paraunas, CEP: 30112-020 Belo Horizonte, MG, Brazil.

0301-9268/$ – see front matter © 2012 Elsevier B.V. All rights reserved.
http://dx.doi.org/10.1016/j.precamres.2012.08.007

1. Introduction

The Gurupi Belt, in northern Brazil, is a Neoproterozoic-Early Cambrian orogen developed in the south-southwestern margin of the São Luís cratonic fragment (Fig. 1A). The cratonic fragment is regarded as part of a major Paleoproterozoic orogen that included part of the Rhyacian-aged Eburnean belts of the West-African Craton (Fig. 1B), and that has been left in the South American continent after the breakup of the Pangea supercontinent (Torquato and Cordani, 1981; Lesquer et al., 1984; Klein and Moura, 2008). Much of the exposed southeastern portion of the Gurupi Belt is composed of Paleoproterozoic (Rhyacian) rocks that are interpreted to be the reworked margin of the São Luís cratonic fragment, representing the external domain of the orogen (Fig. 1C). The exposed internal domain is composed especially of the metasedimentary Gurupi Group (Fig. 1C), which probably represents a Mesoproterozoic–Neoproterozoic passive margin (Costa, 2000; Klein and Lopes, 2011), and much of the domain may be concealed beneath the widespread Phanerozoic sedimentary cover (Almeida et al., 1976; Brito Neves et al., 1984; Cordani et al., 1984; Hasui et al., 1984; Klein et al., 2005a, 2005b).

Several bodies of granitoids have been mapped along two decades in the internal domain of the Gurupi Belt, including gray biotite-bearing monzogranite to granodiorite and leucocratic muscovite-bearing granites (Abreu and Lesquer, 1985; Borges et al., 1988; Pastana, 1995; Costa, 2000). These granitoids occur, in general, as isolated plutons within the younger metasedimentary Gurupi Group. Some of these granitoids have already been dated, mostly based on the single zircon Pb-evaporation technique (Klein et al., 2005b; Palheta et al., 2009), indicating that magmatic events took place around 2.16–2.14 Ga and 2.10 Ga. These events have been related, respectively, to accretionary and collisional phases of a protracted Rhyacian orogeny that built up the São Luís cratonic fragment (Klein et al., 2005a, 2005b; Klein and Moura, 2008; Palheta et al., 2009; Klein and Lopes, 2011).

Recent field mapping undertaken by the Geological Survey of Brazil (Klein and Lopes, 2011, in press), supported by high-resolution airborne geophysics, showed the existence of other bodies of similar muscovite-bearing granites and of quartz syenite (Fig. 1B) that, in previous maps (Pastana, 1995; Costa, 2000), have either been included within undivided basement complexes or overlooked in areas where supracrustal sequences crop out.

Since granitoids and their source magmas are good indicators of the tectonic setting in which they form and are emplaced, in this paper we integrate field, geochemical, geochronological and Nd isotopic data on different compositional types of granitoids recognized in the basement of the Gurupi Belt in order to investigate and discuss the role of these rocks in the Paleoproterozoic magmatic and crustal evolution of the Gurupi-São Luís region. The results include the establishment of the age of emplacement (and metamorphism, where apply) of the granitoids, the interpretation of the geodynamic setting in which the granitoids have formed, and speculations on the age and composition of the source rocks that have been melted to generate the granitoids.

2. Geological overview

The São Luís cratonic fragment is composed, from the oldest to the youngest unit, of: (1) an island arc-related metavolcano-sedimentary sequence (Aurizona Group, 2240 ± 5 Ma; T_{DM} 2.48 Ga and slightly positive εNd value) that was intruded by (2) shallow granophyric rocks at 2214 Ma and by (3) batholiths and stocks of subduction-related, calc-alkaline granitoids (Tromaí Suite) developed in island arc between 2168 and 2147 Ma and that show juvenile Nd signature; (4) andesite, dacite and subordinately basic volcanic rocks of the Serra do Jacaré volcanic unit of 2164 ± 3 Ma (T_{DM} 2.37 Ga and slightly positive εNd values), formed in mature arc with minor back-arc component; (5) minor calc-alkaline felsic volcanic rocks of the Rio Diamante Formation of 2160 ± 7 Ma with limited Archean inheritance (inherited zircon, T_{DM} 2.31 Ga and slightly positive εNd value) formed in a continental margin; (6) peraluminous, collision-type granites of 2086–2091 Ma and T_{DM} ages of 2.32–2.50 Ga with positive to negative εNd values (Tracuateua Suite); and post-orogenic (7) highly evolved/shoshonitic granite of 2056–2076 Ma (Negra Velha Granite) and (8) isolated felsic volcanic rocks (Rosilha volcanic unit) of 2068 Ma and T_{DM} ages of 2.42–2.50 Ga with slightly negative εNd values (Klein and Moura, 2001; Klein et al., 2005a, 2008, 2009; Palheta et al., 2009). These Paleoproterozoic associations are interpreted as forming part of a Rhyacian orogen that record an accretionary (2240–2150 Ma) and a collisional phase (ca. 2100 Ma) that correlate with similar successions of the Eburnean-Birimian terranes of the West-African Craton (Klein and Moura, 2008).

The Gurupi Belt is a Neoproterozoic-Early Cambrian mobile belt developed in the south-southwestern margin of the São Luís cratonic fragment (Fig. 1). The belt consists of rock units of variable natures with ages ranging from the Archean to the Neoproterozoic-Early Cambrian (Klein et al., 2005b; Palheta et al., 2009). These rock units are NW-SE trending successions that follow the general tectonic orientations in the belt. The limit between the Gurupi Belt and the cratonic area is defined by the Tentugal Shear Zone (Hasui et al., 1984). This shear zone, however, is a structural and geochronological limit not a suture, since rocks on both sides of this structure show the same age and Nd signature (Klein et al., 2005a, 2005b).

Small lenses of the Igarapé Grande Metatonalite are the oldest rocks found so far in the belt, with an age of 2594 ± 3 Ma and inherited zircon of 2662 Ma (zircon Pb-evaporation ages, Klein et al., 2005b). This unit represents fragments of an unknown Archean block that is now part of the basement of the belt. The Paleoproterozoic units include (Fig. 1): (1) foliated to banded orthogneisses of the Itapeva Complex of 2167 ± 3 Ma (T_{DM} ages of 2.22–2.31 Ga and positive εNd values; Klein et al., 2005b), with limited remnants of paragneisses and basic-ultrabasic rocks; (2) batholiths of the same juvenile calc-alkaline granitoids of the Tromaí Intrusive Suite found in the São Luís cratonic fragment and showing variable degrees of deformation in the belt; (3) the 2160 Ma old metavolcano-sedimentary Chega Tudo Formation (T_{DM} ages of 2.20–2.34 Ga and positive εNd values; Klein and Moura, 2001) that hosts most of the gold mineralization in the belt; (4) the siliciclastic Igarapé de Areia Formation younger than 2110 Ma (Teixeira et al., 2007) that resembles the Tarkwa sedimentary sequence of Ghana, West Africa (Klein and Lopes, 2009); (5) hydrothermally altered gabbroic rocks intercalated (intruded?) in the metavolcano-sedimentary Chega Tudo Formation (Klein and Lopes, 2011); (6) biotite-bearing monzogranites and granodiorites of 2159–2085 Ma (T_{DM} ages of 2.21–2.48 Ga and positive to negative εNd values; Costa, 2000; Palheta et al., 2009); (7) several generations of variably deformed peraluminous, muscovite- and biotite-bearing granites with ages around 2100 Ma (T_{DM} ages of 2.09–3.23 Ga and positive to negative εNd values; Pastana, 1995; Costa, 2000; Palheta et al., 2009; Klein et al., 2005b; Klein and Lopes, 2011, in press); and (8) highly evolved granite to quartz-syenite (Klein and Lopes, in press). Units (1) to (5) represent the reworked margin of the São Luís cratonic fragment. Units (6)–(8) are the subject of this paper.

In addition to the reworked cratonic margin and basement units, the Gurupi Belt is also composed of younger units. The metasedimentary Gurupi Group occupies most of the exposed area of the belt (Fig. 1). It consists predominantly of schists of turbiditic origin and metamorphic grade varying from lower greenschist facies to amphibolite facies, and subordinate siltstones, quartzites and conglomerates of very low metamorphic grade (Costa et al., 1996;

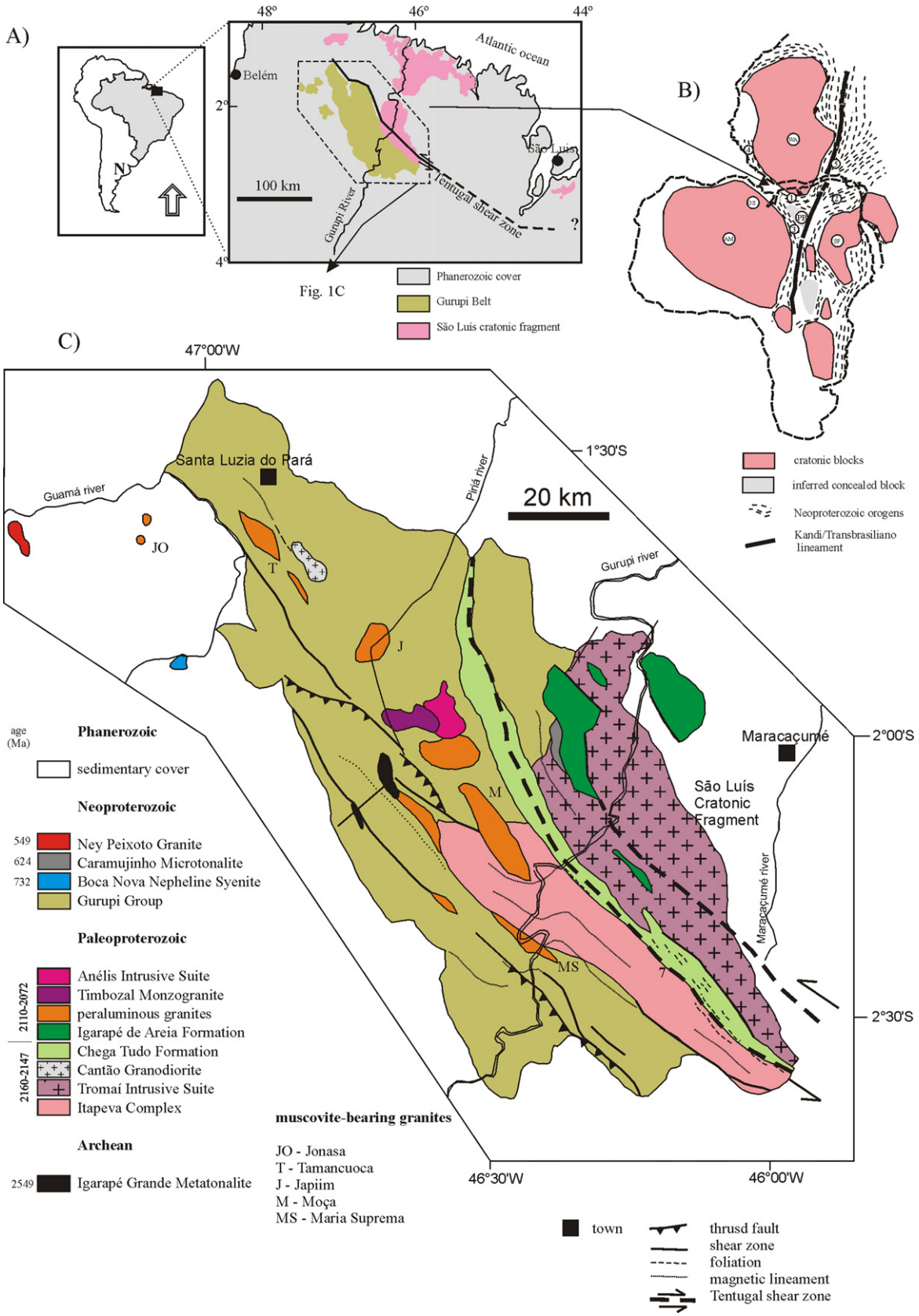

Fig. 1. (A) Location map of the exposed portions of the Gurupi Belt and São Luís Cratonic Fragment. (B) Cartoon not to scale showing the cratons (WA: West African-São Luís Craton; AM: Amazonian Craton; GS: Guiana Shield, SF: São Francisco Craton; PB: Parnaíba block) and mobile belts (1: Gurupi; 2: Borborema; 3: Araguaia; 4: Rockelide; Dahomeyde) of South America and West Africa. Modified from Klein and Moura (2008). (C) Simplified geological map of the Gurupi Belt.

Fig. 2. Outcrop images of the potassic granitoids. (A) Boulder of the equigranular, biotite-bearing Cantão Granodiorite. (B) Rounded microgranular enclave hosted in the Cantão Granodiorite. (C) Coarse-grained, porphyritic variety of the Cantão Granodiorite. (D) Coarse-grained, porphyritic Timbozal Monzogranite intruding the muscovite-bearing Japiim Granite. Contact is rather sharp and some phenocrysts of the enclosing monzogranite appear to have mechanically been included in the intruded granite. (E) Detail of the coarse porphyritic texture, with euhedral to subhedral pink K-feldspar phenocrysts. (F) Rounded quartz-syenite and irregular calc-silicate rock enclaves in the Timbozal Monzogranite. (G) Syenogranite of the Anelis Intrusive Suite with several rounded microgranular enclaves. (H) Detail of an undeformed quartz-syenite of the Anelis Suite. (I) Fine-grained margin of a potassic rock of the Anelis Suite (sy) in sharp contact with a fine-grained mafic rock (maf).

Pastana, 1995; Klein and Lopes, 2011, in press). This sequence is interpreted as a passive margin (Costa et al., 1996) developed from the Mesoproterozoic–Neoproterozoic boundary on and that was inverted (deformed and metamorphosed) during the tectonic events related to the orogenic development of the Gurupi Belt (Klein and Lopes, 2011, in press).

The known Neoproterozoic-Early Cambrian magmatic activity is relatively limited. It is represented by the pre-orogenic alkaline intrusion of the Boca Nova Nepheline Syenite of 732 ± 7 Ma (Klein et al., 2005b), the orogenic Caramujinho Microtonalite of 624 ± 16 Ma (Klein and Lopes, 2011), and the collision-type peraluminous Ney Peixoto Granite of 549 ± 4 Ma (Palheta et al., 2009).

3. Granitoid types

Broadly, three major compositional groups of granitoids are considered below: (1) biotite-bearing, high-K granitoids, (2) highly evolved, alkalic granitoids, and (3) muscovite-bearing granites. Within these groups, eight different bodies of granitoids are investigated here (Fig. 1). The biotite-bearing rocks include the Cantão Granodiorite and the Timbozal Monzogranite; the evolved granitoids are included in the Anelis Intrusive Suite; and the muscovite-bearing rocks comprise the Moça, Maria Suprema, Japiim, Tamancuoca granites, and the Jonasa Granodiorite. The exact shape of some plutons and the relationships with their host rocks are not yet fully understood because of the intense weathering that affected the region. Most of the bodies have been shaped with the help of high-resolution airborne geophysics. Therefore, rock sampling has been more or less effective, depending on the availability of exposures. In this regard, only one exposure of the Jonasa Granodiorite (the Jonasa quarry) is addressed here and we are aware about the pitfalls of assuming this exposure as representative of the unit.

3.1. Cantão Granodiorite

The Cantão Granodiorite has originally been described by Borges et al. (1988). It crops out in the northwestern portion of the Gurupi Belt (Fig. 1B) and consists of light gray biotite-bearing granodiorite and subordinate monzogranite and syenogranite with whitish and greenish tonalities when altered. The rock is medium grained and both equigranular and inequigranular with subordinate porphyritic varieties have been identified. No significant tectonic fabric is observed and microgranular enclaves and cloths of mafic minerals are common features (Fig. 2A–C).

The rocks are composed of quartz (23–42%), plagioclase (13–52%), microcline (11–42%), and biotite (2–14%). Sericite, chlorite, epidote, prehnite and calcite occur as alteration minerals

over the feldspars and/or biotite, whereas titanite, zircon, apatite, allanite and opaque minerals are accessory phases. Micrographic and myrmekitic intergrowths are a common feature; the plagioclase shows concentric zoning and the subordinate porphyritic varieties have phenocrysts of microcline.

3.2. Timbozal Monzogranite

The Timbozal Monzogranite crops out in the central portion of the Gurupi Belt (Fig. 1B) and has previously been considered as a granodioritic facies of the two-mica Japiim Granite (Costa, 2000; Palheta et al., 2009). In fact, the Timbozal Monzogranite intruded the muscovite-bearing Japiim Granite (Fig. 2D). The distinctive feature of the Timbozal Monzogranite is its coarse-grained porphyritic character (Fig. 2D and E). The rocks are gray, the phenocrysts of K-feldspar and plagioclase show random distribution, whereas the matrix is discontinuously foliated. Syn-plutonic dykes are common and decimeter-wide enclaves/xenoliths of alkali feldspar quartz syenite (Anelis type), monzogranite and of calc-silicate sedimentary rocks have been identified (Fig. 2F).

The petrographic composition is rather restricted. Monzogranite (with a granodioritic matrix) is by far the main type, whereas granodiorite and quartz-monzonite are subordinate. The rocks are composed of quartz (17–38%), K-feldspar (9–32%), plagioclase (20–50%) and biotite (2–13%). Hornblende has been detected only in one sample (1%) and muscovite is subordinate (<3%) and is not ubiquitous. Titanite, apatite, allanite, zircon and opaque minerals are accessory phases, whereas chlorite, sericite and carbonate minerals are alteration phases. The main microscopic textures are granular, granular hipidiomorphic and porphyritic. Quartz shows weak undulose extinction; the K-feldspar displays mesoperthite exsolutions and micrographic intergrowth; the plagioclase shows oscillatory zoning and myrmekitic intergrowth; biotite defines a well-developed to discontinuous foliation and may locally be accompanied by muscovite.

3.3. Anelis Intrusive Suite

The Anelis Intrusive Suite crops out in the central portion of the Gurupi Belt (Fig. 1) and has been recognized by Klein and Lopes (in press). The suite has a distinctive geophysical signature when compared with the surrounding units, showing the highest Th contents among the studies granitoids. The magnetic pattern is rather disturbed and characterized by low magnetic values.

The suite is composed of pinkish to grayish, inequigranular, locally porphyritic, medium- to coarse-grained rocks, which are massive to foliated and show centimeter-wide microgranular enclaves (Fig. 2G) and enclaves of amphibolite. Where present, the tectonic fabric is defined by planar orientation of feldspars and mafic minerals. Augite-bearing quartz syenite (Fig. 2H), biotite- or hornblende-bearing syenogranite and hornblende-bearing quartz monzonite are the petrographic types. The rocks are composed of microcline (40–45%), quartz (15–25%), plagioclase (10–15%), augite (up to 25%), hornblende (15–25%), biotite (2–5%) and titanite (up to 3%). Pyroxene-bearing varieties do not contain amphibole or biotite and may contain tourmaline. Opaque minerals, zircon, allanite, apatite and epidote are accessory phases, whereas sericite and chlorite are alteration minerals.

The inequigranular types show anhedral granular texture, whereas the porphyritic varieties show anhedral microcline and amphibole or pyroxene phenocrysts set in a quartzo-feldspathic matrix. Microstructures include quartz with undulose extinction, oriented microcline with local development of subgrains, localized zones of intense dynamic recrystallization and mylonitic fabric.

3.4. Moça Granite

The Moça Granite has been mapped by Klein and Lopes (2011) in the central portion of the Gurupi Belt (Fig. 1). Other poorly characterized bodies occurring both to the west and to the east may belong to the same unit. The main pluton is relatively well defined as a roughly sigmoidal shape, which is elongated to the NW-SE direction (Fig. 1). The Moça Granite intruded into gneisses of the Itapeva Complex, as indicated by granitic veins crosscutting the gneisses near the contact between the two units. The granite is pink, equigranular, medium grained (Fig. 3A) and bear subconcordant quartz veins and pegmatite. The preferred orientation of elongated muscovite and biotite flakes defines the tectonic foliation that strikes to N20°–60°W and dips steeply to the northeast.

Muscovite- and biotite-bearing syenogranite and monzogranite are the predominant types and granodiorite is subordinate. These rocks are composed of quartz (25–42%), microcline (15–43%), plagioclase (19–55%), muscovite (3–10%) and biotite (1–10%). Apatite, zircon and opaque minerals are accessory phases. Under the microscope the mylonitic fabric is defined by lens-shaped plagioclase and microcline porphyroclasts involved by a foliated and locally kinked quartz-feldspar-mica-bearing matrix. Small recrystallized grains of K-feldspar and myrmekitic overgrowths occur in the margins of the porphyroclasts. Quartz crystals are elongated and well-developed mica flakes show weak undulose extinction.

3.5. Maria Suprema Granite

The Maria Suprema Granite has been defined by Pastana (1995) and according to Klein et al. (2005b), it consists of discontinuous meter-thick sheets and layers of leucocratic muscovite- and biotite-bearing syenogranites and monzogranites that intruded parallel to the foliation of the Paleoproterozoic basement gneisses of the Itapeva Complex (Fig. 3B). The rocks are pink, medium-grained and structurally vary from mylonitic to porphyroclastic, schistose and gneissic. The foliation strikes to N45°–60°W and dips moderately to steeply (>60°) both to SW and NE, suggesting that a strike slip regime affected the unit.

The mineralogy consists of quartz (30–45%), K-feldspar (15–29%), plagioclase (15–36%), muscovite (7–25%) and biotite (3–15%). Zircon, apatite, opaque minerals, titanite and allanite are accessory phases, and Pastana (1995) has also described the presence of andalusite. Chlorite and epidote are alteration minerals. The mylonitic texture is defined by plagioclase porphyroclasts set in a recrystallized quartzo-feldspathic matrix and wrapped by stretched and oriented flakes of muscovite and biotite. Quartz grains are also elongated, sometimes forming long stripes.

3.6. Japiim Granite

The Japiim Granite crops out in the central-northwestern portion of the Gurupi Belt (Fig. 1). The pluton is composed of medium- to coarse-grained, equigranular to inequigranular biotite- and muscovite-bearing monzogranite (Fig. 3C, D) and subordinate syenogranite and granodiorite. The rocks are leucocratic with pink to light gray colors and are variably foliated, but rarely massive, depending on their relationships with structures. Quartz, quartzo-feldspathic and granitic veins and dykes are ubiquitous and show variable orientations.

The rocks are composed of quartz (25–36%), microcline (16–40%), plagioclase (15–31%), muscovite (7–15%), and biotite (<1–5%). Zircon, apatite and opaque minerals are accessory phases and chlorite and epidote are alteration minerals. Microscopic features include subhedral to anhedral granular textures, which are often modified by solid state intra-crystalline deformation, such as formation of subgrains, undulose extinction of quartz and

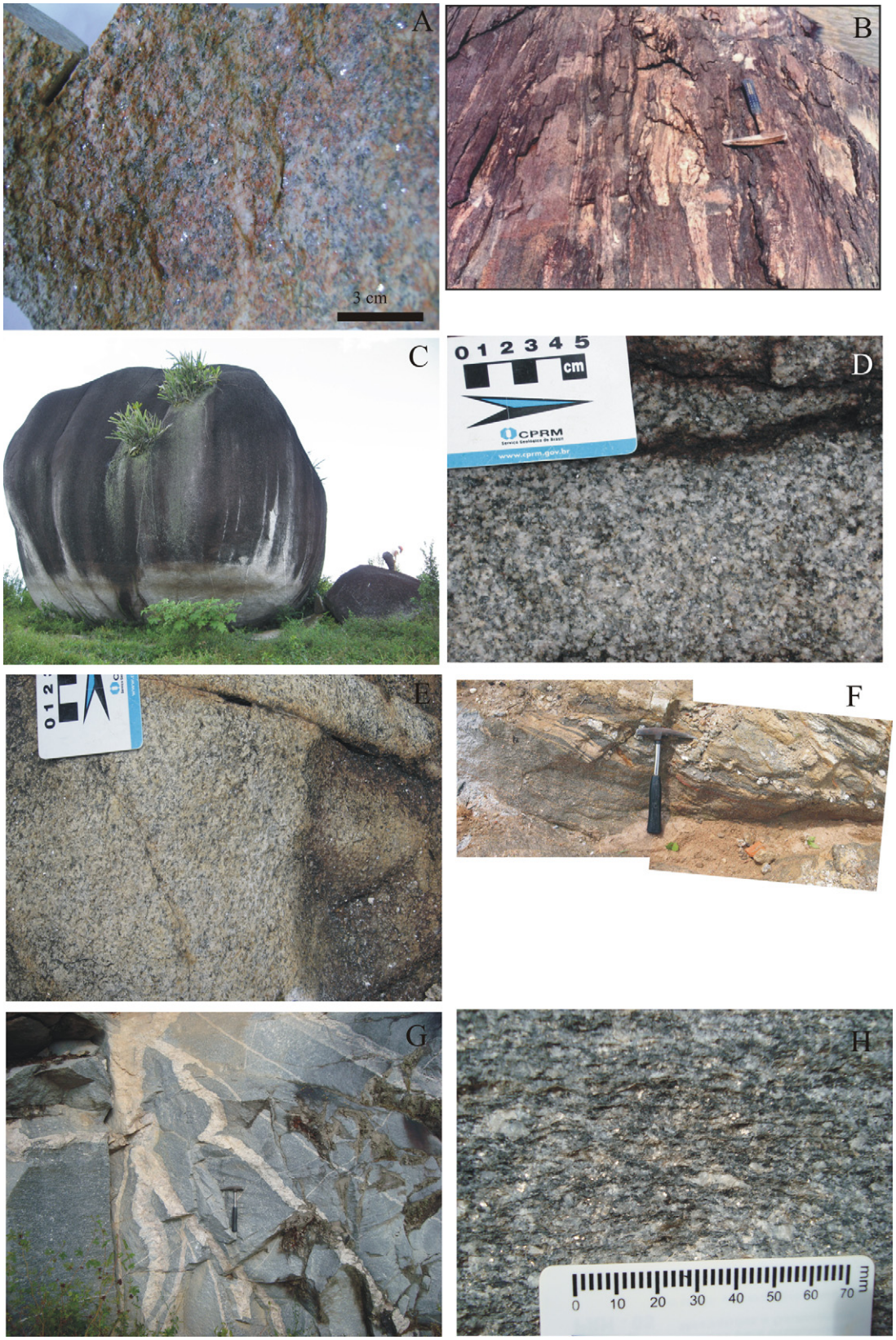

Fig. 3. Outcrop images of the muscovite-bearing granites. (A) Hand sample of the Moça Granite. (B) Sheets of the Maria Suprema Granite intruding basement gneiss of the Itapeva Complex. (C) Boulders and (D) hand sample of the Japiim Granite, with bright small muscovite (ms) crystals. (E) Weakly deformed and (F) banded/gneissose varieties of the Tamancuoca Granite. (G) Jonasa Granodiorite intruded by granitic pegmatites. (H) Detail of the granodiorite showing orientation of quartz and mica (bright white crystals). (For interpretation of the references to color in the text, the reader is referred to the web version of the article.)

muscovite, and kink bands. Muscovite and biotite are oriented, defining the foliation of the rocks and indicate formation under equilibrium.

3.7. Tamancuoca Granite

The Tamancuoca Granite has been recognized by Klein and Lopes (in press) and crops out in the northwestern portion of the Gurupi Belt. The rocks are fine- to coarse-grained and leucocratic with whitish gray, pinkish and yellowish colors (Fig. 3E). They are in general foliated, with the foliation defined by the orientation of muscovite flakes, and oriented generally to NW-SE. Gneissose varieties have also been detected (Fig. 3F). The bodies of this muscovite- and biotite-bearing granite are probably tectonically intercalated within the metasedimentary rocks of the Gurupi Group.

Monzogranite is the predominant compositional type, with subordinate occurrences of syenogranite and granodiorite. The rocks are composed of quartz (24–34%), microcline (15–40%), plagioclase (12–41%), muscovite (7–24%) and biotite (1–4%). Zircon, apatite, and opaque minerals are accessory phases, while chlorite and epidote are alteration minerals. The microscopic textures are fine- to medium-grained granular with interlobed or polygonal contacts, and lepidoblastic. Quartz and microcline are commonly stretched and oriented. Subgrains and undulose extinction in quartz indicate dynamic deformation. Myrmekite, perthite and antiperthite overgrowths are also common features.

3.8. Jonasa Granodiorite

Jonasa is a granitoid described by Costa (2000) on the basis of a single very large outcrop (the Jonasa quarry) that occurs in the north-western portion of the Gurupi Belt. Field relationships are unknown since the granitoid is covered by a thin layer of more or less consolidated Cenozoic sediments (Fig. 1). The Jonasa Granodiorite is a gray (Fig. 3G), leucocratic to mesocratic, medium-grained and foliated to banded rock. The foliation and banding strike to N25°W, with moderate to steep dips to SW. Palheta et al. (2009) reported low (<10°) to moderate (25°) angle stretching lineation of quartz plunging, respectively, to 325°–353° Az (strike parallel) and 263°–267° Az (dip parallel). Timing relationships between these two directions are unknown. Concordant and discordant centimeter- to meter-thick veins and pockets of quartz, granite and garnet- and beryl-bearing pegmatite are common (Fig. 3H).

The granodiorite is composed of quartz (27–48%), plagioclase (30–44%), microcline (10–19%), biotite (5–13%) and muscovite (2–12%). Titanite, apatite and zircon are accessory phases and sericite and chlorite are alteration minerals. The contacts between quartz and feldspar minerals are sinuous and defined by the elongation of micas. Myrmekite has been observed.

4. Geochemistry

The analytical procedures are described in Appendix A and representative whole rock geochemical results for the studied granitoid units are given in Tables available as supplementary data files.

4.1. Cantão Granodiorite and Timbozal Monzogranite

Both the Cantão and Timbozal units have moderate to high SiO_2 concentrations varying from 61 to 72 wt.%, and are high-K_2O calc-alkaline rocks (Fig. 4A, B). The K_2O/Na_2O ratios are lower than 1.4, but they are less variable in the Cantão Granodiorite. The sum of $Fe_2O_3 + MgO + TiO_2$ ranges from 2.1 to 6.0 wt.%, which is consistent with the presence of biotite contents in the rocks. However, the Timbozal rocks are weakly peraluminous, whereas Cantão shows more variation in the alumina saturation index, being weakly to

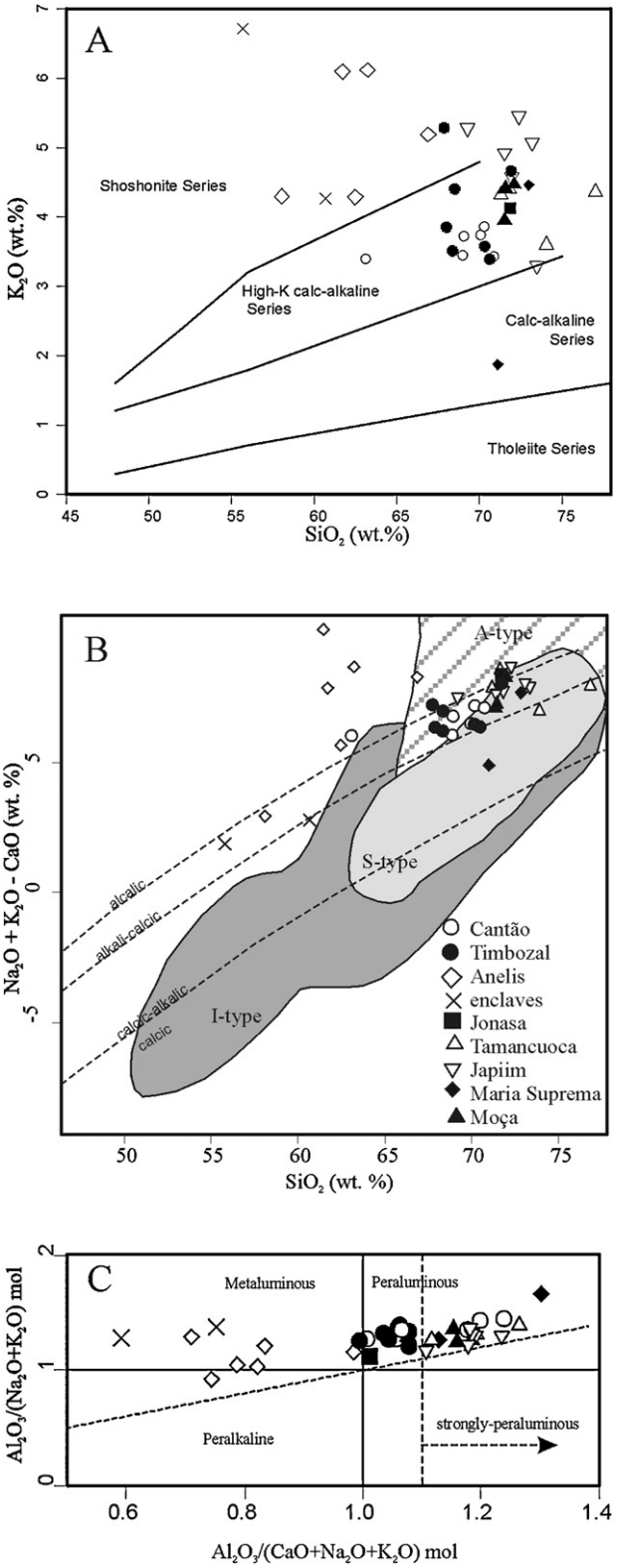

Fig. 4. (A) SiO_2 versus K_2O diagram of Peccerilo and Taylor (1976). (B) SiO_2 versus $K_2O + Na_2O$ – CaO diagram of Frost et al. (2001) with the fields of S-, I- and A-type granites for comparison. (C) Lower part of the A/CKN versus A/NK (Shand diagram) plot for the studied granitoids.

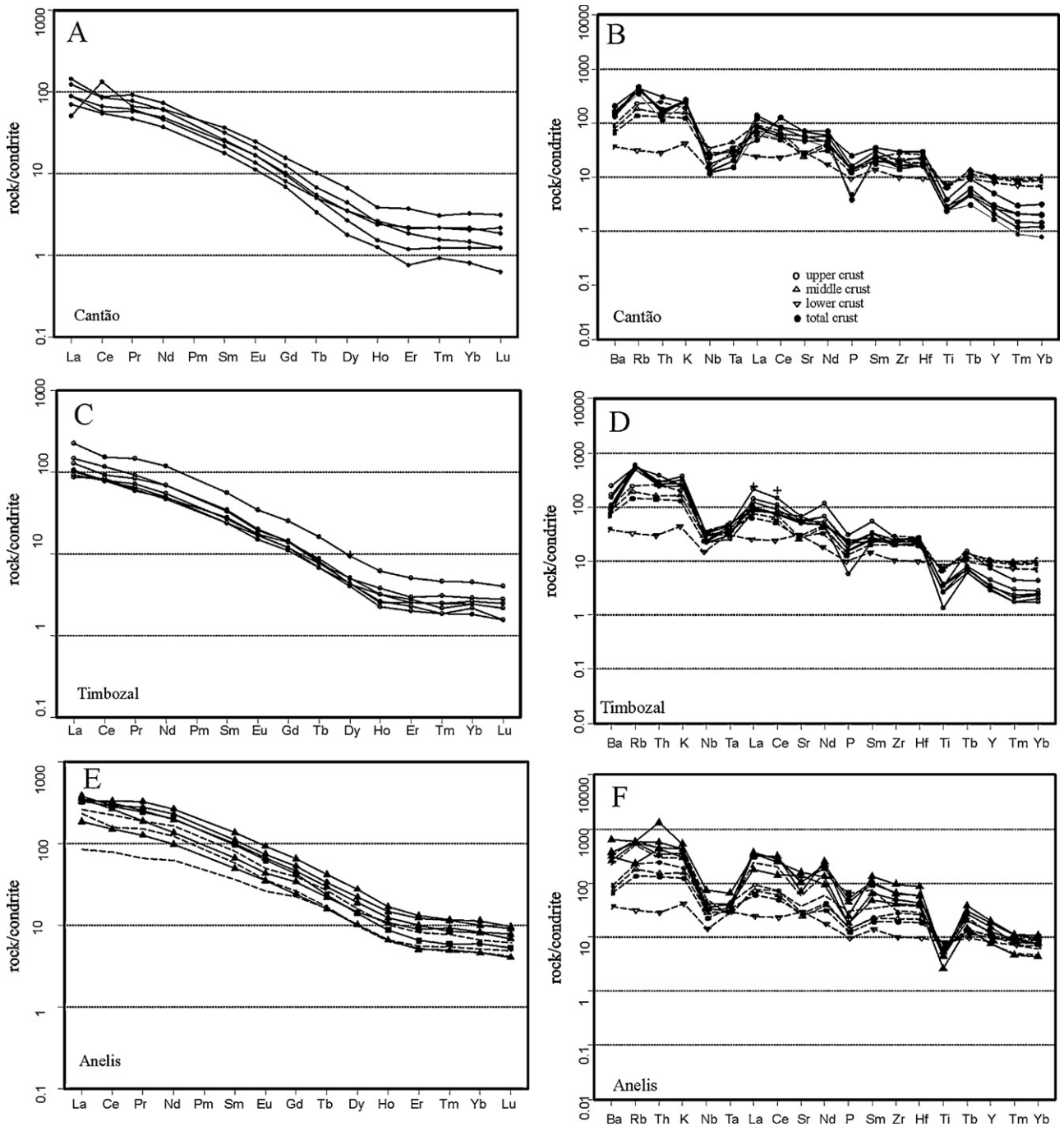

Fig. 5. Chondrite-normalized REE (Boynton, 1984) and multi-element (Thompson, 1982) plots for the potassic granitoids. Crustal values (Rudnick and Gao, 2005) are shown for comparison. Dashed lines in plots E and F are from enclaves found in the Timbozal Monzogranite.

strongly (A/CKN > 1.1) peraluminous (Fig. 4C). In average, the Timbozal Monzogranite is slightly richer in SiO_2, CaO, K_2O, TiO_2 and P_2O_5 than the Cantão Granodiorite.

The Rb/Sr ratios are relatively low and similar in the two granitoids (0.2–0.4), but the Ba/La and Sr/Y ratios are a higher in the Cantão Granodiorite than in the Timbozal Monzogranite, indicating that Cantão is somewhat more differentiated than Timbozal. In general, the Zr, Y and Nb concentrations are higher in the Timbozal unit. Cantão and Timbozal show similar average Nb/Ta ratios of 12.8 and 12.4, respectively, which are similar to that of the continental crust (Rudnick and Gao, 2005).

The rare earth elements (REE) show fractionation between the light and heavy elements (Fig. 5). The fractionation is larger and more variable in the Cantão Granodiorite (La_n/Yb_n = 16–100) than in the Timbozal Monzogranite (La_n/Yb_n = 32–56), but Timbozal shows somewhat more elevated REE contents. The Eu/Eu* ratios of 1.0–1.1 and 0.9–1.0 in the Cantão and Timbozal types, respectively, indicate that plagioclase fractionation was not an effective process in the genesis of the magmas. The chondrite normalized extended multi-element diagrams are also similar for the two granitoid types (Fig. 5). They show enrichment of large ion litophile elements (LILE) in relation to the high field strength elements (HFSE), strongly negative Nb–Ta and P anomalies (which are more pronounced in the Cantão Granodiorite), and negative Ti anomalies. However, the Timbozal type is a little bit more enriched in both HFSE and LILE when compared to the Cantão type, having also more variable

elemental concentrations. In addition, the weak Sr anomaly and the Ti anomaly are slightly more pronounced in the Timbozal type. Coupled Nb–Ta–Ti depletions may be ascribed to the influence of fluids derived from a subducting slab on arc magmas or to the presence of amphibole and titaniferous phases in the residue (Drummond and Defant, 1990; Jahn et al., 2008).

4.2. Anelis Intrusive Suite

The Anelis suite presents a rather restricted SiO_2 content (58.1–66.9 wt.%) and are rich in alkalis, with very high K_2O (>4.3 wt.%) and $Na_2O + K_2O$ (>7.7 wt.%) concentrations (Fig. 4A, B), and with K_2O/Na_2O ratios in general >1 wt.%. In chemical classification diagrams the rocks plot in the fields of syenite, quartz syenite and quartz monzonite (figures not included). The rocks are weakly metaluminous and locally evolve toward weakly peralkaline composition (Fig. 4C). They also show high Rb, Sr, Ba, Zr, Y, and Nb concentrations.

The REE concentrations are the highest among the studied units. The elements show strong enrichment in relation to the chondrite and strong fractionation between light and heavy elements, which is given by La_n/Yb_n ratios of 29–44. The element distribution in different samples is rather parallel indicating a same parental magma source (Fig. 5E). The absence of significant Eu anomaly ($Eu/Eu^* = 0.9–1.0$) suggests that plagioclase has not been significantly fractionated, or if fractionation has occurred it has been compensated by fractionation of other phases.

The trace element pattern is characterized by strong LILE enrichment and moderate HFSE enrichment when compared to the chondrite (Fig. 5F), indicating fractionation between the two groups of elements. Pronounced Nb–Ta, P, and Ti, and weak Sr negative anomalies are characteristic features. The high average Nb/Ta ratio of 17.8 is higher than crustal values and similar to the chondritic and Bulk Silicate Earth values (Jochum et al., 2000; Rudnick and Gao, 2005). As a whole, the Anelis Suite has characteristics that are similar to those of shoshonitic series and A-type granites

4.3. Muscovite-bearing granites

The rocks of the Tamancuoca and Japiim granites show SiO_2 concentrations between 69 and 77 wt.%, whereas the other muscovite-bearing granitoids show more restricted variation in the SiO_2 content (71–73 wt.%). The Al_2O_3 content is rather similar among all the granitoids, ranging from 13.8 to 16.4 wt.%. All rocks have high K_2O contents and the K_2O/Na_2O ratios are generally lower than 1.0, except for the Japiim granite that has ratios up to 1.6. The sum of $Fe_2O_3 + MgO + TiO_2$ ranges from 1.4 to 3.6 wt.%, which is consistent with the low contents of mafic minerals. According to the alumina saturation index the rocks plot in the field of the strongly peraluminous, S-type granites (Fig. 4A). Only the sample of the Jonasa type plots in the limit of the metaluminous and peraluminous fields.

The REE patterns (Fig. 6) are characterized by strong but variable fractionation between light and heavy elements. The heaviest elements, from Er to Lu, show a rather flat pattern, and approach chondritic values. The Japiim Granite shows greater variation when compared to the other types of muscovite-bearing granites, especially in the light elements pattern. The Eu anomaly is in general weak ($Eu/Eu^* = 1.2–0.8$), except for a few samples of the Jonasa, Japiim and Maria Suprema granites that show Eu/Eu^* ratios of 0.6–0.4.

The chondrite normalized multi-element diagrams (Fig. 6) show broadly similar patterns, for all granitoid units, which are characterized by strong LILE enrichment and weak enrichment to depletion of HFSE, given by very variable La_n/Yb_n ratios of 7–247. Moça and Maria Suprema show the highest fractionation, pronounced Nb–Ta negative anomalies, and weak to moderate P and Ti negative anomalies, which are more pronounced in the Maria Suprema type. Differences presented by the other granite types are the weaker fractionation, the absence of Ta and P anomalies, and the more pronounced Ti negative anomaly in the Tamancuoca and Japiim types. In addition, the Japiim Granite shows very variable elemental enrichments when compared to the other types.

As a whole, the trace-element patterns indicate the presence of crustal components in the magma genesis (e.g., Taylor and McLennan, 1985). The P anomaly suggests fractionation of apatite during differentiation and the Nb and Ti anomalies might reflect the presence of Fe–Ti oxides among the liquidus fractionated phases (Foley and Wheller, 1990). Average Nb/Ta ratios of 5.6–9.4 (except for the Maria Suprema Granite, but in this case the Ta concentrations are exactly the detection limit) are quite lower that the continental crust ratio and approximate that of the lower crust (Rudnick and Gao, 2005). Such low values might have been produced by fluid fractionation during magma generation (Münker, 1998; Dostal and Chatterjee, 2000).

5. U–Pb LA-ICP-MS geochronology

The Cantão, Timbozal, Jonasa and Maria Suprema granitoids have already been dated (Klein et al., 2005b; Palheta et al., 2009). The reported crystallization ages of these granitoids are, respectively, 2163 ± 4 Ma, 2084 ± 5 Ma, 2072 ± 8 Ma (single zircon Pb-evaporation), and 2100 ± 12 Ma (zircon U–Pb TIMS).

In this paper we present for the first time U–Pb zircon LA-ICP-MS data for the Moça, Tamancuoca and Japiim granites and for the Anelis Intrusive Suite. We also present U–Pb data for the previously dated Jonasa Granodiorite. The summary of isotopic results are presented in Tables available as supplementary data files, and the analytical procedures are described in Appendix A. Analyses were preceded by Cathodoluminescence (CL) and/or Backscattered Electron (BSE) imaging to check the internal structures of individual zircon crystals and to select suitable spots for laser ablation.

5.1. Anelis Intrusive Suite

An augite-bearing syenogranite was selected for dating (EK92). Zircon crystals show very variable shapes and internal structures (Fig. 7A). Most of the crystals are prismatic, with aspect ratio of 2:1 to 5:1, and show oscillatory zoning. Many show corrosion and resorption features, and fractures are ubiquitous.

The isotopic results of 29 spots on 21 zircon grains yielded strong and variable discordance and the $^{207}Pb/^{206}Pb$ apparent ages have high analytical uncertainties. All Th/U ratios are >0.16 and fall within the magmatic range. Excluding ten crystals with high common lead contents and three crystals with high analytical uncertainties the remaining isotope ratios define a regression line that intercepts the concordia at 2106 ± 53 Ma and 405 ± 200 Ma (Fig. 7B). Progressively reducing the number of more discordant crystals (improving the MSWD parameter), several arranges give upper intercept ages between 2123 and 2139 Ma and lower intercept ages between 555 and 767 Ma, both with very high uncertainties (figures not included). Further reduction to ≤13% discordant ratios returns upper and lower intercept ages of 2123 ± 59 Ma and 679 ± 390 Ma, respectively. The least discordant result (3%) obtained in the core of crystal 37 gives a concordia age of 2100 ± 21 Ma (Fig. 7B).

The presence of enclaves of quartz syenite in the Timbozal Monzogranite and the possible intrusion relationships with the Cantão Granodiorite bracket the age of the Anelis suite between 2084 ± 5 Ma and 2163 ± 4 Ma. Therefore, we interpret the age of 2100 ± 21 Ma as the best approximation of the emplacement age

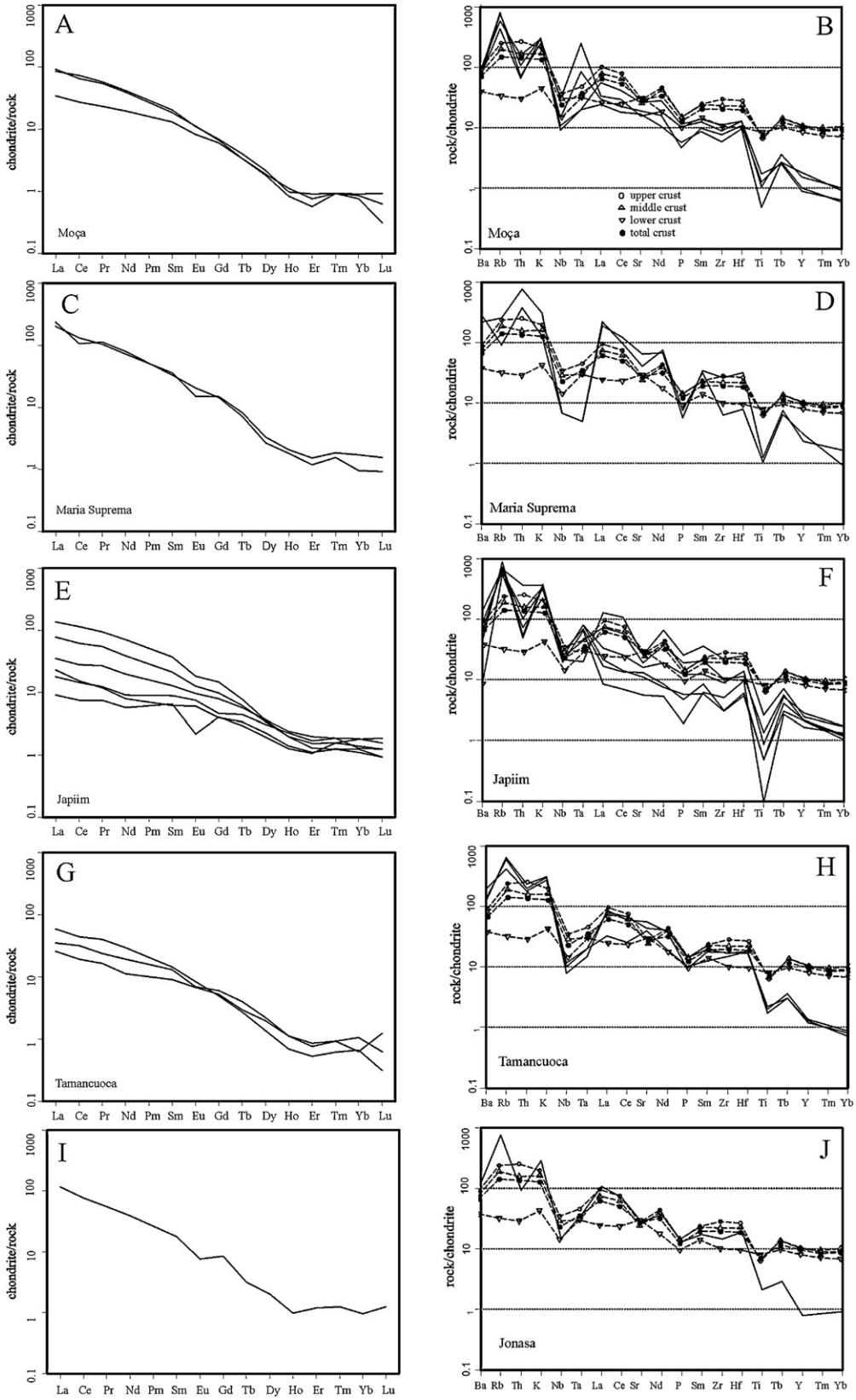

Fig. 6. Chondrite-normalized REE (Boynton, 1984) and multi-element (Thompson, 1982) plots for the muscovite-bearing granitoids. Crustal values (Rudnick and Gao, 2005) are shown for comparison.

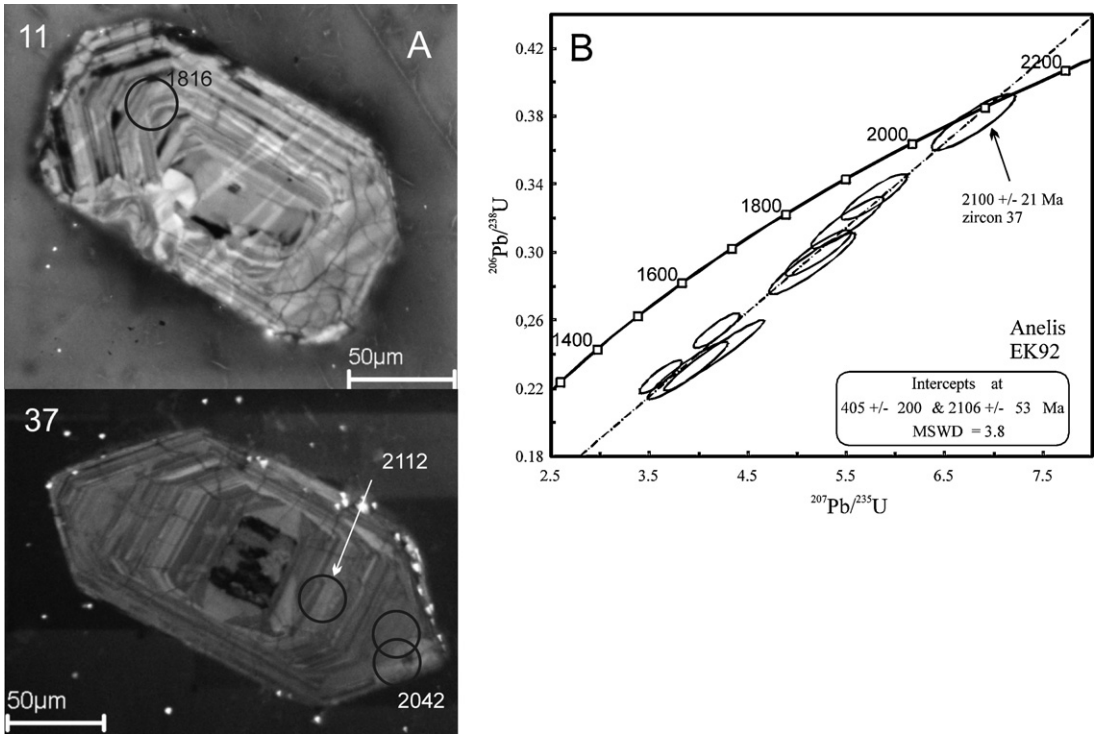

Fig. 7. (A) Cathodoluminescence images of zircon crystals of the Anelis Intrusive Suite, with spot location (circles); numbers correspond to zircon number in supplementary tables; apparent $^{207}Pb/^{206}Pb$ ages in Ma. (B) Concordia plot for sample EK92 of the Anelis Intrusive Suite.

of the Anelis Intrusive Suite. The lower intercept ages, despite the large analytical errors, are interpreted as produced by lead loss during a Neoproterozoic-Early Cambrian tectono-thermal overprint.

5.2. Moça Granite

Sample EK70 is a biotite- and muscovite-bearing monzogranite from the type locality of the unit. Forty spots were done on 19 zircon grains and many of them show highly discordant isotope ratios and/or high common Pb contents. Furthermore, CL and BSE images revealed complex internal structure and different morphologies for the studied crystals (Fig. 8A). Based on these aspects and on the isotopic results, several age populations are distinguished, and examples of each population are as follows.

Crystal 9 shows a fragment of a magmatic-textured core with oscillatory zoning and a thin euhedral and zoned overgrowth. Between these two domains there is evidence of resorption, which is more visible in the lower part of the image (Fig. 8A). The magmatic core of this crystal has a slightly discordant (2.6%) age of 2649 ± 25 Ma. The core of crystal 33 is also magmatic-textured and the isotope ratios yield a concordant age of 2316 ± 5.5 Ma. Both ages are interpreted as inheritance.

The cores of crystals 1 and 43 show discordance of 6 and 4%, respectively, low Th/U ratios and rather similar isotopic compositions that show reverse discordance and variable apparent ages. Crystal 1 has a rounded and relatively homogeneous and structureless core (in BSE image) and a thin, diffusely zoned to spongy overgrowth (Corfu et al., 2003; Sapienza et al., 2007) also with low Th/U ratio. Crystal 43 is multifaceted and this morphology is typical of metamorphic zircon (Hoskin and Schaltegger, 2003), surrounded by a thin, euhedral and zoned overgrowth (Fig. 8A). The two cores yield an imprecise age of 2198 ± 75 Ma. Despite the relatively small discordance, the apparent ages are very different and the analytical errors are large and the meaning, if any, of this age remains uncertain.

The isotopic ratios obtained in the cores of eight oscillatory-zoned crystals vary from concordant to less than 10% discordant, but are not collinear. The two crystals (38, 39) with $^{207}Pb/^{206}Pb$ apparent ages higher than 2.2 Ga produce an upper intercept age of 2242 ± 62 Ma. Despite the large error, it appears that the grains belong to an older source (and are interpreted as inheritance), because excluding these two crystals, the remaining six crystals produce an upper intercept age of 2162 ± 19 Ma (MSWD = 1.5). The two groups of ages barely overlap within the limits of analytical errors. The two more concordant zircons (7 and 28) of the younger group produce a concordia age of 2149 ± 15 Ma. If crystal 19 is included, despite the large apparent errors, an indistinguishable age of 2151 ± 14 Ma is obtained. The idiomorphic to sub-idiomorphic morphologies of the cores, the presence of idiomorphic overgrowths (probably melt-precipitated outer rims with fine-scale oscillatory zoning) and of resorption features given by irregular zones with bright CL response between core and overgrowth (e.g., crystals 19, 41 and 44), and the presence of xenocrystic cores (zircon 7) indicate that these core ages also represent inheritance. Furthermore, within this group, crystal 13 shows three domains (Fig. 8A): (1) a dark gray core with concentric zoning, (2) a relatively thick and structureless and highly luminescent intermediate domain with radial fracturing probably indicating expansion by metamictization, and (3) a dark rim/overgrowth. Core and rim of this crystal yielded $^{207}Pb/^{206}Pb$ apparent ages of 2145 Ma (Th/U = 0.25) and 2108 Ma (Th/U = 0.02), respectively.

Several crystals have magmatic cores, Th/U > 0.1, and isotope ratios that correspond to younger apparent ages. Excluding the spots with large errors, four spots on crystals 16, 26 and 29, yielded upper and lower intercept ages of 2088 ± 28 Ma and 699 ± 899 Ma, respectively. Further reduction, with the exclusion of the more discordant spot on crystal 16, yielded a more precise, but indistinguishable within errors, upper intercept age of 2099 ± 19 Ma (Fig. 8B).

Spots on the rims of four crystals (1, 11, 13 and 44) with low (<0.1) Th/U ratios show variable isotope ratios, and

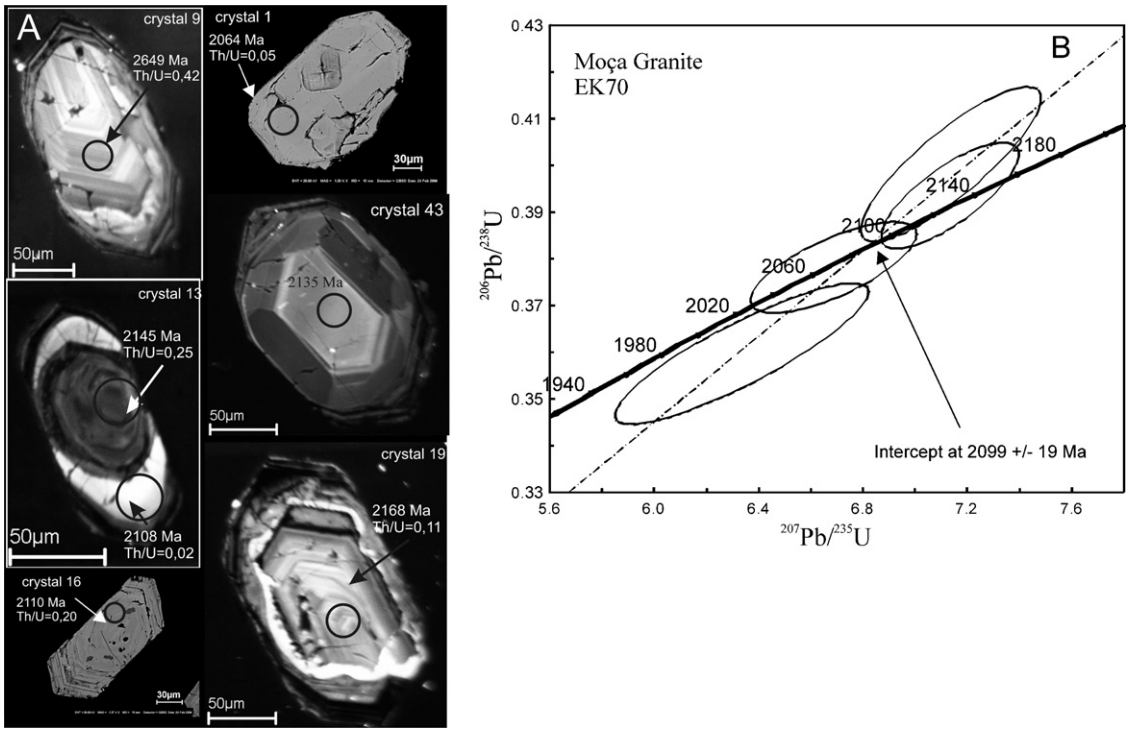

Fig. 8. (A) Cathodoluminescence and backscattered electron images of zircon crystals of the Moça Granite, with spot location (circles); numbers correspond to zircon number in supplementary tables; apparent $^{207}Pb/^{206}Pb$ (or concordia, where apply) ages in Ma. (B) Concordia plot for sample EK70 of the Moça Granite.

discordance between 0.5 and 15%. Together, the four crystal rims yielded an upper intercept age of 2096 ± 31 Ma (MSWD = 2.3). Despite the large error and poor fit, this age is indistinguishable, within errors, from the age presented above, found on the "younger cores". Excluding the analyses with larger discordances and errors, the best fit is obtained using the three less discordant spots that yielded an intercept age of 2081 ± 36 Ma (MSWD = 0.35).

All mentioned ages of 2088 ± 28, 2099 ± 19, 2096 ± 31, and 2081 ± 36 overlap within analytical uncertainties, which means that they are all the same age. Hence, we regard the more precise age of 2099 ± 19 Ma to be the best approximation among the data for the crystallization age of the Moça Granite.

5.3. Japiim Granite

The sample selected for U–Pb dating (EK146) is a biotite- and muscovite-bearing syenogranite collected near the type locality of the unit in the Japiim Village. The isotopic results and apparent ages combined with morphologic and BSE and CL images of the analyzed zircon crystals allowed several groups to be separated.

Crystals 25 and 26 show complex internal structure and apparent $^{207}Pb/^{206}Pb$ ages of 2614 and 2545 Ma, respectively. Crystal 25 is elongated, rounded (detrital?), fractured and possibly corroded in one of the faces. The internal structure is characterized by a rounded core showing magmatic zoning and overgrowth that passes abruptly to a structureless and irregular zone of high luminescence (Fig. 9A). Part of the outer portion shows

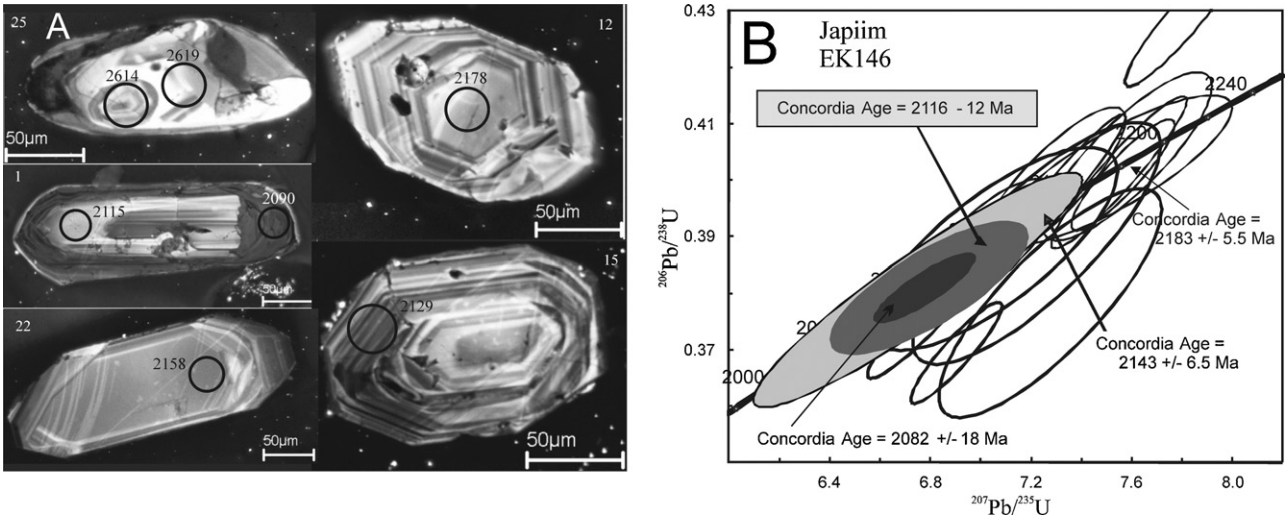

Fig. 9. (A) Cathodoluminescence images of zircon crystals of the Japiim Granite, with spot location (circles); numbers correspond to zircon number in supplementary tables; apparent $^{207}Pb/^{206}Pb$ ages in Ma. (B) Concordia plot for sample EK146 of the Japiim Granite showing the various concordant ages (see interpretation in the text).

sponge-like texture. The two crystals represent inheritance from Archean sources. Crystal 25 has a low Th/U ratio of 0.03 that could represent a metamorphic age or alteration (see Section 7).

The group formed by grains 4, 6, 9, 10, 12, 15, and 22 shows prismatic crystals, with or without defined pyramids, and some are rounded. All the cores show oscillatory zoning. The four more concordant data from the cores (crystals 4, 12, 15, and 22) allow us to calculate a concordia age of 2183 ± 5.5 Ma, which is interpreted as inheritance. The Th/U ratios of the cores vary between 0.18 and 0.51 and are consistent with a magmatic origin. The rims show variable intensity of corrosion and signs of metamictization and are either zoned (9, 10, 12, 15) or homogeneous (4, 22). Despite differences in their internal structure, the rims show similar isotope ratios and the more concordant ones yielded a concordia age of 2143 ± 6.5 Ma. The Th/U ratios of the rims are consistent with a magmatic origin. These ages are also interpreted as inheritance.

Crystals 1, 2, and 36 are prismatic with short pyramids and their cores show magmatic zoning, some fractures, inclusions and possible resorption (Fig. 9A). In some areas the contact between rim and core is not clearly defined. Other areas show a sharp contact between the core and well-developed, 10–60 μm-thick overgrowths. The Th/U ratios of these crystals fall within the magmatic range and the isotope ratios of crystals 1 and 2 are concordant allowing us to calculate a concordia age of 2116 ± 12 Ma (Fig. 9B), which is interpreted to be the crystallization age of the Japiim Granite.

There is a close similarity in the low Th/U (<0.1) and Pb/U ratios of the rims of crystals 1 and 24. The isotope ratios of the rims of the two crystal plot on the concordia curve and define an age of 2082 ± 18 Ma (Fig. 9B). Even considering analytical errors, this age does not overlap with the crystallization age (see interpretation in Section 7).

Crystals 20 and 23 show younger concordant ages both in the cores and rims. Core and rim ages are of 1512 ± 22 Ma and 1406 ± 8 Ma for crystal 20, and 1860 ± 21 Ma and 1921 ± 8 Ma for crystal 23, respectively. Only the rim of crystal 20 has a low Th/U ratio (outside the magmatic range). This crystal is rounded and shows structureless and irregular bright and dark gray portions in cathodoluminescence image, with a thin bright rim. Probably the U–Th–Pb system behaved open for these crystals due to metamictization and/or metamorphism, but the cause of the concordance remains uncertain. The fact that the age of the rim of crystal 23 is older than the age of the core supports the disturbance hypothesis. Similar situations have been described for undeformed volcanic rocks of the São Luís cratonic fragment (Klein et al., 2009) and the Kaapvaal Craton (Poujol et al., 2005). In these cases the authors related the younger concordant ages to Pb loss associated with partial resorption and reprecipitation of the crystals during known younger magmatic events. In the present study region, however, magmatic events of these ages (1.4–1.9 Ga) are not known to date and only detrital zircon crystals recovered from a conglomerate have been found, yielding ages around 1500 Ma (Lucas et al., 2009). The source of these detrital crystals is still uncertain. Alternatively, the age of 1512 ± 22 Ma could represent the crystallization age of the granite, and all older ages would represent inheritance. However, this is not consistent with the intrusion relationship with the Timbozal Granite.

5.4. Tamancuoca Granite

The sample selected for U–Pb dating is a muscovite-bearing monzogranite (EK51) sampled at the type area of the unit. The analyzed zircon crystals have variable sizes and shapes. The crystals consist of long to short prisms; some are rounded, with two pyramids. BSE images show that most of the crystals have corroded margins. The cores of crystals 2 and 17 are subrounded or subhedral, more or less fractured and show light gray BSE colors and oscillatory zoning. The rims of these crystals form more or less regular overgrowths with spongelike features. Crystal 13 shows a subrounded, fractured and apparently structureless xenocrystic core and an irregular overgrowth (Fig. 10A).

The isotopic results show variable discordance and some crystals have high common lead contents (f206 > 3%) and discordance over 70%. Excluding these crystals, three groups of crystals can be observed (Fig. 10B). Crystals 10, 12 and 16 have $^{207}Pb/^{206}Pb$ apparent ages between 2217 and 2243 Ma and represent inheritance. The isotopic ratios of the majority of the crystals have $^{207}Pb/^{206}Pb$ apparent ages between ~2100 and 2155 Ma and plot along a regression line that intercepts the concordia at 2141 ± 7 Ma and 140 ± 43 Ma, with MSWD of 1.4 (Fig. 10B). Four crystals with $^{207}Pb/^{206}Pb$ ratios around 0.12 yield a discordia that intercepts the concordia at 2079 ± 12 Ma and 242 ± 54, with MSWD of 0.45. Zircon 1 from this group is concordant, with an age of 2081 ± 9 Ma, which overlaps the discordia age, and both may represent the best approximation to the crystallization age of the Tamancuoca Granite. The lower intercept ages appear to be meaningless, because they do not fit in any known event in the region, and probably represent variable Pb-loss. All the analyzed rims show high common lead concentrations and discordance, very variable apparent ages, and $^{206}U/^{238}Pb$ and $^{207}U/^{235}Pb$ ratios tending to younger ages (Fig. 10B).

5.5. Jonasa Granodiorite

The zircon crystals from sample ML1A are mostly prismatic, ranging from 100 μm to 250 μm in the longest axis, and with aspect ratio ranging from 1:4 to 1:1. As shown by BSE images (Fig. 11A), the crystals are complex, often metamictic, rich in inclusions, with overgrowths and, in places, with zoned cores and porous and fractured rims. Some have ghost texture. Most of the cores show oscillatory zoning and a few are structureless. All but grain 34 present high Th/U ratios, which are consistent with the magmatic field.

Among the selected crystals, it was possible to complete the analysis of 17 cores. Analytical data from four crystals that presented high errors and/or high common Pb contents were not used in age calculations. In addition, the isotope ratios of the rims could not be determined due to the instability of the signal associated with the high concentration of U and common Pb.

As a whole, the isotopic ratios show variable discordance ranging from 3.5% to 44.4%, mostly >10%. The analytical points form a relatively poor alignment that suggests lead loss in the present. A closer observation of the concordia plot identifies two groups that for almost parallel alignments (Fig. 11B). However, no difference in the morphology and internal structure of the zircon crystals from the two groups was observed. Data from six crystals of the older group show some scatter. The regression through these data provided the upper intercept of 2169 ± 33 Ma (MSWD of 3.1), interpreted as inheritance. Isotopic ratios of the younger group of seven crystals show a better alignment (MSWD = 0.96) and include concordant data. These seven crystals define an upper intercept of 2142 ± 9 Ma (Fig. 11B), which is assumed to better represent the intrusion age of the Jonasa Granodiorite.

6. Nd isotopes

Sm–Nd isotope compositions have been determined in whole rock samples of the Cantão, Moça, Japiim, Tamancuoca, Timbozal and Anelis units. Analytical procedures (Gioia and Pimentel, 2000) are described in Appendix A. The results are presented in Table 1 along with previously published data. Depleted mantle

Table 1
Available whole rock Sm–Nd data for the Rhyacian granitoids of the basement of the Gurupi Belt.

Sample/unit	Age (Ma)	Sm (ppm)	Nd (ppm)	Sm/Nd	f(Sm/Nd)[a]	$^{147}Sm/^{144}Nd$	$^{143}Nd/^{144}Nd$	2σ (10^{-6})	εNd(0)	εNd(t)	T_{DM} (Ga)ss	T_{DM} (Ga)ds	References
Cantão													
EK26	(2163)	10.15	41.85	0.242	−0.25	0.1466	0.511564	10	−20.9	−7.1	–	2.92	1
C01	2163[E]	4.34	25.11	0.173	−0.47	0.1045	0.511279	–	−26.5	−0.9	2.48	–	2
C02	(2163)	4.49	26.13	0.172	−0.47	0.1038	0.511454	–	−23.1	+2.7	2.21	–	2
Moça													
EK70	2099[L]	4.884	29.90	0.163	−0.50	0.0987	0.511397	6	−24.2	+2.2	2.19	–	1
EK74	(2099)	3.572	22.37	0.159	−0.51	0.0965	0.511293	9	−26.2	+2.3	2.28	–	1
Japiim													
J02	(2116)	5.66	27.32	0.207	−0.36	0.1253	0.511757	–	−17.2	+2.2	2.22	–	2
J03	(2116)	3.69	13.67	0.269	−0.17	0.1632	0.512005	–	−12.4	−3.3	3.23	2.62	2
Tamancuoca													
EK48	(2101)	3.115	13.68	0.227	−0.30	0.1376	0.511755	13	−17.2	−1.3	2.60	–	1
EK51	2101[L]	3.550	19.82	0.179	−0.45	0.1082	0.511376	13	−24.6	−0.8	2.42	–	1
MSuprema													
EK25B	2100[T]	7.15	41.63	0.171	−0.47	0.1039	0.511390	8	−24.3	+0.7	2.30	–	3
Anelis													
EK88	(2100)	29.522	170.98	0.172	−0.47	0.1044	0.511290	7	−26.3	−2.6	2.46	–	1
EK92	2100[L]	32.034	178.59	0.179	−0.45	0.1084	0.511479	7	−22.6	+0.1	2.27	–	1
Timbozal													
EK131A	(2084)[E]	5.369	27.86	0.192	−0.41	0.1165	0.511393	18	−24.3	−2.8	2.58	–	1
EK135	(2084)[E]	6.420	36.51	0.175	−0.46	0.1063	0.511452	19	−23.1	+1.1	2.27	–	1
Jonasa													
TAG02	(2140)[L]	2.37	13.96	0.170	−0.48	0.1026	0.511304	–	−26.02	−0.2	2.40		2
TAG05	(2140)	2.89	13.50	0.214	−0.34	0.1292	0.511885	–	−14.7	+3.9	2.09	2.14	2

ss: single stage; ds: double stage (recalculated from original data – see text for explanation).
Age column: ages in brackets are the estimated age based on dated samples of the same unit; E: single zircon Pb-evaporation; L: zircon U–Pb LA-ICP-MS; T: zircon ID-TIMS.
Key to Nd data references: 1 – this work, 2 – Palheta et al. (2009), 3 – Klein et al. (2005b).
[a] Normal range: [f(Sm/Nd)] −0.60 to −0.35; $^{147}Sm/^{144}Nd$ 0.08–0.13.

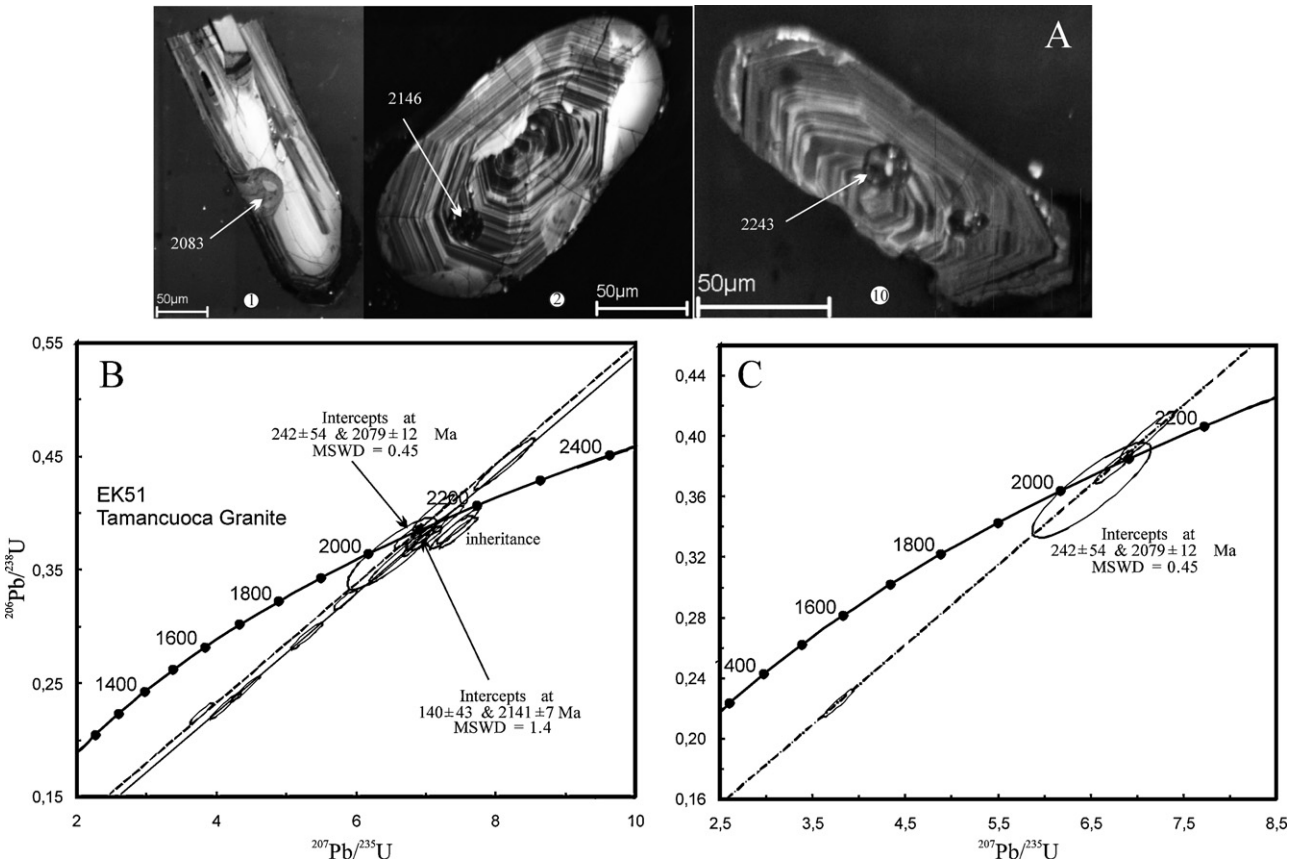

Fig. 10. (A) Cathodoluminescence electron images of zircon crystals of the Tamancuoca Granite, with spot location (pit – circles); numbers correspond to zircon number in supplementary tables; apparent $^{207}Pb/^{206}Pb$ ages in Ma. (B) Concordia plot for sample EK51 of the Tamancuoca Granite, showing the results for all analyzed spots. (C) Concordia plot showing the isotopic ratios used in the calculation of the crystallization age.

(T_{DM}) model ages were calculated to the crystallization age according to the single-stage model of DePaolo (1981). In two cases (Cantão and Japiim units), the results show $^{147}Sm/^{144}Nd$ ratio and/or fractionation factor [f(Sm–Nd)] outside the normal range for felsic rocks that have not undergone chemical fractionation. In these cases the double-stage model of DePaolo (1981) was tentatively used, with the second stage starting at the crystallization age.

The Moça Granite shows T_{DM} model ages of 2.19 and 2.28 Ga, and εNd values of +2.2 and +2.3. These results indicate that Paleoproterozoic sources predominate in the genesis of the granitic magma and that Archean sources have been strongly limited. In fact, only one Archean zircon has been detected during the U–Pb work.

Regarding the Japiim Granite, the analyzed sample furnished a result that is not suitable for model age calculation. The same apply to sample J03 of Palheta et al. (2009), and the model age of 3.23 Ga is

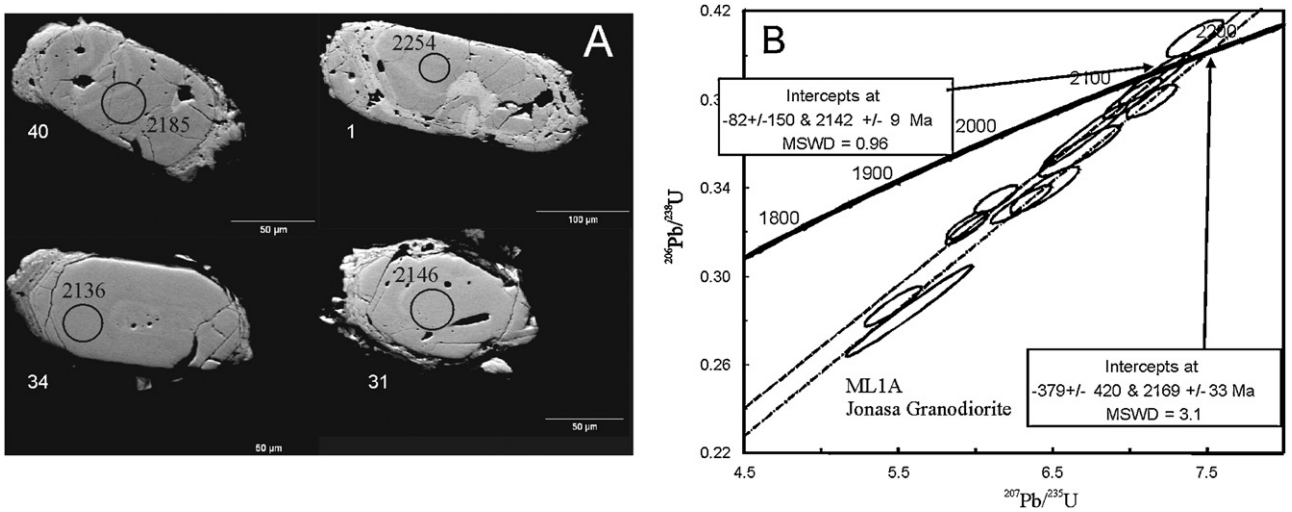

Fig. 11. (A) Backscattered electron images of zircon crystals of the Jonasa Granodiorite, with spot location (circles); numbers correspond to zircon number in supplementary tables; apparent $^{207}Pb/^{206}Pb$ ages in Ma. (B) Concordia plot for sample ML1A of the Jonasa Granodiorite, showing the two age populations (crystallization age and inheritance).

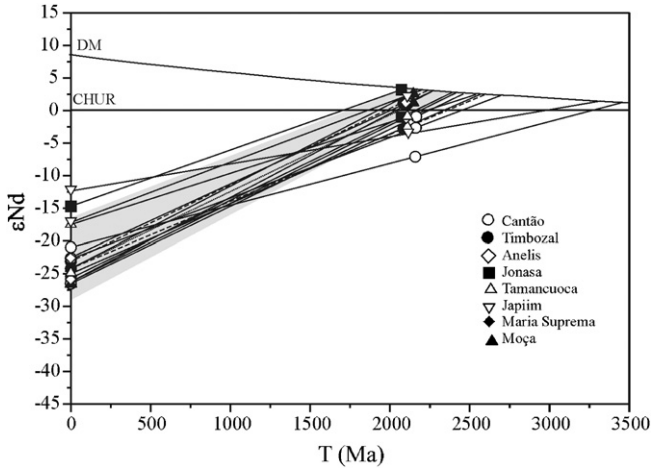

Fig. 12. Time vs. εNd diagram for the granitoids discussed in this study. The shaded area corresponds to the Nd evolution of the Rhyacian juvenile crust of the São Luís cratonic fragment, the "São Luís crust", as defined by Klein et al. (2005a).

not relevant. Recalculation of this age using the double-stage model yielded a model age of 2.62 Ga, which combined with the age of 2.22 Ga from Palheta et al. (2009) and the moderately positive to moderately negative εNd values indicate mixed Paleoproterozoic and Archean sources for the protoliths of the Japiim Granite.

The results for the two samples of the Tamancuoca Granite yielded model ages of 2.42 and 2.6 Ga with slightly negative εNd values. The samples from the Anelis Intrusive Suite returned model ages of 2.27 and 2.46 Ga, with εNd values of +0.1 and −2.6, respectively. Similarly, the Timbozal Granodiorite have model ages of 2.27 and 2.58 Ga, with εNd values of +1.1 and −2.8, respectively. In all these cases, mixed Paleoproterozoic and Archean sources are indicated as sources for the protoliths of these units.

The εNd versus time diagram (Fig. 12) shows the evolution of the Nd system in the studied plutonic rocks. The diagram also shows the field of evolution of the Paleoproterozoic "São Luís crust", as defined by Klein et al. (2005a), which represents the juvenile Paleoproterozoic (2240–2150 Ma) rocks of the São Luís cratonic fragment. Accordingly, based only on the Nd evolution, one can observe that the Maria Suprema, Moça, Jonasa and Anelis units were formed predominantly from sources compatible with the São Luís crust. On the other hand, the Cantão and Tamancuoca granitoids have older sources, whereas the Japiim and Timbozal granitoids appear to have mixed sources that include both the São Luís and older crusts.

7. Discussion

Table 2 summarizes the geochronological and Nd isotope data and Table 3 shows a summary of the main petrographic and geochemical characteristics of the Paleoproterozoic granitoids from the basement of the Gurupi Belt. The main issues for discussion are as follows.

7.1. The age of the Jonasa Granodiorite

The Jonasa Granodiorite had already been dated by different techniques. Klein and Moura (2003) used the whole rock Rb–Sr systematics and obtained an age of 2018 ± 61 Ma (MSWD = 1.9) with an initial $^{87}Sr/^{86}Sr$ ratio of 0.7034, which is close to the upper mantle composition (Faure, 1986). Klein and Moura (2003) also obtained an age of 525 ± 20 Ma from an internal Rb–Sr isochron (MSWD = 7) calculated from the isotopic ratios of biotite, muscovite, K-feldspar and whole rock. The authors interpreted the older and younger

Table 2
Summary of geochronological and Nd isotope data of Paleoproterozoic granitoids of the Gurupi Belt.

Granitoid unit	Magmatic series	Tectonic phase	Inheritance (Ma)	Crystallization age (Ma)	Low Th/U rim ages (Ma)	Lower intercept ages (Ma)	Isochrone age (Ma)	T_{DM} (Ga)	εNd(t)	Reference
Cantão	HKCA	Pre-collision		2163 ± 4				2.21, 2.48	+2.7, −0.9	1
Jonasa	P	Pre-collision	2446 ± 7	2142 ± 9			525 ± 20	2.09, 2.40	+3.2, −1.1	1, 2, 4
			2387 ± 5							
			2374 ± 6							
			2325 ± 10							
			2169 ± 33							
Anelis	ALK	Late orogenic		2100 ± 21		679 ± 390		2.27, 2.46	+1.2, −1.4	2
Timbozal	HKCA	Late/post orogenic	2351 ± 12	2084 ± 5				2.27, 2.61	+1.1, −2.8	1, 2
Moça	SP	Collision	2649 ± 25	2110 ± 16	2098 ± 19	545 ± 290		2.19, 2.28	+2.2, +2.3	2
			2195 ± 16		2064 ± 12					
			2151 ± 14							
Japiim	SP	Collision	2614	2116 ± 14	2082 ± 18			2.22, 3.23	+1.9, −3.4	2, 1
			2545							
			2147 ± 8							
Tamancuoca	SP	Collision	2217–2243	2079 ± 12				2.42, 2.60	−0.8, −1.3	2
			2141 ± 7							
Maria Suprema mobilized	SP	Collision		2100 ± 12	2080 ± 3	358 ± 20		2.30	+0.7	3
		Collision (migmatization)	2580–2607	2092 ± 20						4

Key to references: 1 – Palheta et al. (2009), 2 – this work, 3 – Klein et al. (2005b), 4 –Klein and Moura (2003).
HKCA: high-K_2O calc-alkaline; ALK: alkalic; SP: strongly peraluminous; P: peraluminous.

Table 3
Summary of the characteristics of Rhyacian granitoid units from the basement of the Gurupi Belt.

Main groups types	Potassic granitoids			Two mica leucogranites				
	Cantão	Timbozal	Anelis	Tamancuoca	Japiim	Moça	Maria Suprema	Jonasa
Petrographic types (QAP)	Granodiorite (syenogranite, monzogranite)	Monzogranite (granodiorite, quartz-monzonite)	Quartz-syenite, syenogranite, quartz-monzonite	Monzogranite (syenogranite, granodiorite)	Monzogranite (syenogranite, granodiorite)	Syenogranite, monzogranite (granodiorite)	Syenogranite (granodiorite)	Granodiorite
Mafic mineralogy	Biotite (2–14%)	Biotite (2–13%) amphibole (<1%)	Pyroxene (<25%), amphibole (15–25%), biotite (2–5%), titanite (<3%)	Biotite (1–4%)	Biotite (<1–5%)	Biotite (1–10%)	Biotite (3–15%)	Biotite (5–13%)
Aluminous minerals		Muscovite (<3)		Muscovite (7–24%)	Muscovite (7–15%)	Muscovite (3–10%)	Muscovite (7–25%)	Muscovite (2–12%)
Accessory mineralogy	Titanite, apatite, zircon, allanite, opaque	Titanite, apatite, zircon, allanite, opaque	Zircon, allanite, apatite, epidote, opaque (tourmaline)	Apatite, zircon, opaque	Apatite, zircon, opaque	Apatite, zircon, opaque	Titanite, apatite, zircon, allanite, opaque	Titanite, apatite, zircon,
Texture and structure	Medium-grained equigranular, inequigranular	Very coarse-grained porphyritic	Medium- to coarse-grained, inequigranular to porphyritic, massive to foliated	Foliated	Medium- to coarse-grained, equigranular, inequigranular	Medium-grained, equigranular, foliated to mylonitic	Medium-grained, mylonitic to porphyroclastic	Medium-grained, foliated to banded
SiO_2 (wt.%)	63–71	61–72	58–67	71–77	69–73	72	71–73	72
K_2O (wt.%)	3.4–3.6	3.4–5.3	4.3–7.6	4.3–4.4	3.3–5.5	3.9–4.5	1.9–4.5	4.1
K_2O/Na_2O	0.7–0.9	0.7–1.4	0.9–1.5	0.9–1.0	0.6–1.6	0.9–1.0	0.4–1.1	0.8
Alumina saturation index	Weakly to strongly peraluminous	Weakly peraluminous	Weakly metaluminous to weakly peralkaline	Strongly peraluminous	Strongly peraluminous	Strongly peraluminous	Strongly peraluminous	Weakly peraluminous
$Fe_2O_3 + MgO + TiO_2$ (wt.%)	2.6–6.0	2.1–5.5	4.0–13.2	1.4–2.1	1.4–3.6	3.9–4.5	1.9–4.5	2.3
Rb (ppm)	122–163	174–206	80–202	155–265	196–308	146–225	32–90	268
Sr	551–817	581–787	809–1860	182–311	67–303	466–662	481–763	335
Ba	905–1434	563–1679	1790–4366	437–609	59–960	864–1333	1515–1985	840
Zr (ppm)	94–202	138–214	238–646	40–76	21–153	102–118	43–178	100
Y	3.3–9.9	5.8–23.3	15–40	1.8–3.1	3.3–5.7	2.4–2.7	4.7–6.1	1.6
Nb	4.0–8.8	7.6–11.9	7.3–25.9	3.2–10.4	6.9–9.8	11.9–25.4	43.2–47.8	23.5
ΣETR (ppm)	102–186	143–409	278–640	37–83	17–204	54–126	233–238	136
La/Yb(n)	16–100	32–56	29–56	34–90	7–78	45–108	116–247	121
Eu/Eu*	1.0–1.1	0.9–1.0	0.9–1.0	0.8–1.0	0.4–1.2	0.9–1.0	0.6–0.9	0.6
Ba/La	25–91	18–38	19–42	33–59	21–76	35–80	24–27	23
Sr/Y	82–173	55–108	20–106	59–173	20–62	179–276	79–162	213
Rb/Sr	0.2–0.3	0.2–0.4	<0.1–0.2	0.7–1.5	0.8–2.9	0.2–0.5	0.1	0.8
Nb/Ta	11.0–14.7	9.3–15.7	14.6–19.9	2.1–9.5	5.3–18.8	8.8–10.3	24	7.1
Age (Ma)	2163 ± 4	2084 ± 5	2100 ± 21	2079 ± 12	2116 ± 12	2099 ± 19	2100 ± 12	2142 ± 9
T_{DM} (Ga)	2.21–2.92	2.27–2.58	2.27–2.48	2.42–2.60	2.22–2.62	2.19–2.28	2.3	2.14–2.40
εNd(t)	+2.7 to −7.1	+1.1 to −2.8	+0.1 to −2.6	−0.8 to −1.3	+2.2 to −3.2	+2.2 to +2.3	+0.7	+3.9 to −0.2

Rock types in brackets are subordinate; references in the text.

ages as representing, respectively, the crystallization and metamorphism/deformation ages of the Jonasa Granodiorite.

Palheta et al. (2009) using the single zircon Pb-evaporation technique, obtained a mean age of 2072 ± 3 Ma (from two crystals out of >20), correctly interpreted to be the minimum age of crystallization of the granitoid, in keeping with the fundamentals of the method (Kober, 1986). The authors also detected inherited crystals with ages between 2325 and 2446 Ma.

It is noteworthy that the samples dated in the studies above and in our study were collected in the same outcrop of the Jonasa quarry. Considering that the granodiorite underwent metamorphism and deformation, that many zircon crystals show metamictization (also reported by Palheta et al., 2009), and that variable discordance has been demonstrated by our data, it is probable that the age reported by Palheta et al. (2009) reflects Pb loss and is likely meaningless. Therefore, we understand that the age of 2142 ± 9 Ma obtained by the U–Pb method represents better the crystallization age of the Jonasa granodiorite.

We do not have a clear explanation for the inherited crystals found by Palheta et al. (2009), with ages around 2.3 Ga, and that were not detected in our study. Although the six data-points used to calculate the upper intercept of 2169 Ma, which was interpreted as inheritance, may not represent a unique population, yet their $^{207}Pb/^{206}Pb$ apparent ages are younger than 2260 Ma and cannot be correlated with the data found by Palheta et al. (2009).

7.2. Lower intercept ages

Four investigated units present lower intercept ages between 358 and 679 Ma with large analytical errors. These errors may have been produced by regression of data belonging to different populations or, more likely, by variable discordance of the zircons. Nevertheless, they point to isotope disturbance (Pb loss) in younger times, which is interpreted as produced by tectonic and/or magmatic and/or metamorphic events related to the Neoproterozoic-Early Cambrian Brasiliano cycle of orogenies. The disturbance hypothesis is supported by the presence of thin undated rims. The timing of the Neoproterozoic metamorphism in the study region is not yet constrained. Available Rb–Sr and K–Ar mineral and whole rock ages vary between 1000 and 466 Ma (mostly between 580 and 520 Ma – see review in Klein et al., 2005b). The Boca Nova nepheline syenite and the Caramunjinho microtonalite were emplaced at 732 ± 7 Ma (Klein et al., 2005b) and 624 ± 16 Ma (Klein and Lopes, 2011), respectively. These units underwent subsequent metamorphism at amphibolite and greenschist facies conditions, respectively (Lowell and Villas, 1983; Klein et al., 2005b; Klein and Lopes, 2011), and no references to metamorphism is made in the descriptions of the Ney Peixoto Granite of 549 ± 5 Ma (Villas and Sousa, 2007; Palheta et al., 2009). Therefore, the youngest metamorphic event in the study region is estimated to have occurred in the 624–549 Ma interval. Alternatively, more than one metamorphic event may have taken place in the region.

7.3. Ages obtained in low Th/U rims and in multifaceted grains

Low Th/U ratios may result from the selective partitioning of Th and U into the fluid and/or preferential leaching of U relative to Th during amphibolite to granulite facies metamorphism and the consequent recrystallization of new zircon crystals and/or growth of metamorphic rims around pre-existing zircons (Williams and Claesson, 1987; Vavra et al., 1999; Pidgeon et al., 2000; Wu and Zheng, 2004). However, low Th/U ratios in zircon can also be produced by crystallization from Th-poor magmas, leaching of Th by fluids, and are primarily influenced by factors such as element availability within a reaction environment and partitioning of Th and U between zircon and co-existing minerals, melts and fluids (Pidgeon et al., 1998; Geisler et al., 2001; Zinger and Levchenkov, 2003; Harley et al., 2007). Therefore, low Th/U ratios alone are not enough to characterize the metamorphic provenance of zircons.

In this study, we show that significant granitoid magmatism related to anatexis took place in the Gurupi Belt and the presence of low Th/U leucogranitic anatectic mobilized crosscutting gneisses of the Itapeva Complex has been described in Klein and Moura (2003). In consequence, the low Th/U ratios found in several samples are considered here to have been caused by some process related to this relatively large scale anatectic event. Probably, the Rhyacian metamorphism was associated to this event.

7.4. Possible sources for the inherited zircon

Inherited ages were detected in most of the granitoid types and indicate that the source materials for these granitoids came from rocks of several different types and/or ages. Many of them have not been detected in outcropping unites to date.

Archean ages are grouped in two intervals: 2.58–2.54 Ga and 2.65–2.61 Ga. The first one is similar to the age of the unique Archean unit known in the basement of the Gurupi Belt to date, the Igarapé Grande Metatonalite, and the later is similar to the inherited age found in this same unit (2.59 and 2.66 Ga, respectively, Klein et al., 2005b).

The Siderian ages of 2.32–2.39 (2.44) Ga found by Palheta et al. (2009) were obtained by the Pb-evaporation technique and should be confirmed by in situ techniques. Nevertheless, assuming that these ages are meaningful, they represent sources still unknown in the region. Siderian rocks have limited exposures in the Bacajá domain of the Amazonian Craton, about 800 km to the southwest (Vasquez et al., 2008), and in the Médio Coreaú domain of the Borborema Province, about 700 km to the east (Santos et al., 2009).

The ages of 2.21–2.19 Ga are only vestigial in the region. Zircon crystals of 2.19 Ga have been found only as inheritance within 2.15–2.16 Ga gneisses belonging to the Itapeva Complex (Klein et al., 2005b). However, a similar age was obtained in the cores of the two multifaceted grains (especially grain 43) of the Moça Granite and indicates limited presence of source materials that underwent high grade metamorphism at about 2.20 Ga. This event has not been recognized in the Gurupi region so far. However, high grade metamorphism is relatively well defined to have occurred in the neighboring Amazonian Craton at about 2.10–2.07 Ma (Rosa-Costa et al., 2008; Vasquez et al., 2008).

A significant part of the inheritance is of Rhyacian ages of 2.17–2.14 Ga, which are the ages of most of the Paleoproterozoic units found in the São Luís cratonic fragment and its reworked margin (Tromaí Intrusive Suite, Chega Tudo Formation, Itapeva Complex – Klein et al., 2005a, 2005b). If these rocks contributed to the source of the peraluminous granites, terrane exhumation must have occurred in less than 30 Ma. The Archean and Rhyacian ages are also found in the West African Craton (see review in De Kock et al., 2011).

7.5. Origin of the muscovite-bearing granites and leucogranites

The A/CKN ratios >1.1 define the Rhyacian-aged muscovite-bearing granites and leucogranites of the basement of the Gurupi Belt as strongly peraluminous rocks (Sylvester, 1998). This feature, the presence of muscovite and biotite, and the abundance of inherited zircon populations with a relatively complex age spectra, are also consistent with the characteristics of S-type granites. On the other hand, S-type granites commonly have preserved enclaves/xenoliths of metasedimentary rocks, which have not been observed in the granites addressed in this study. Furthermore, these rocks also show characteristics of (highly-) fractionated granitoids (Fig. 13).

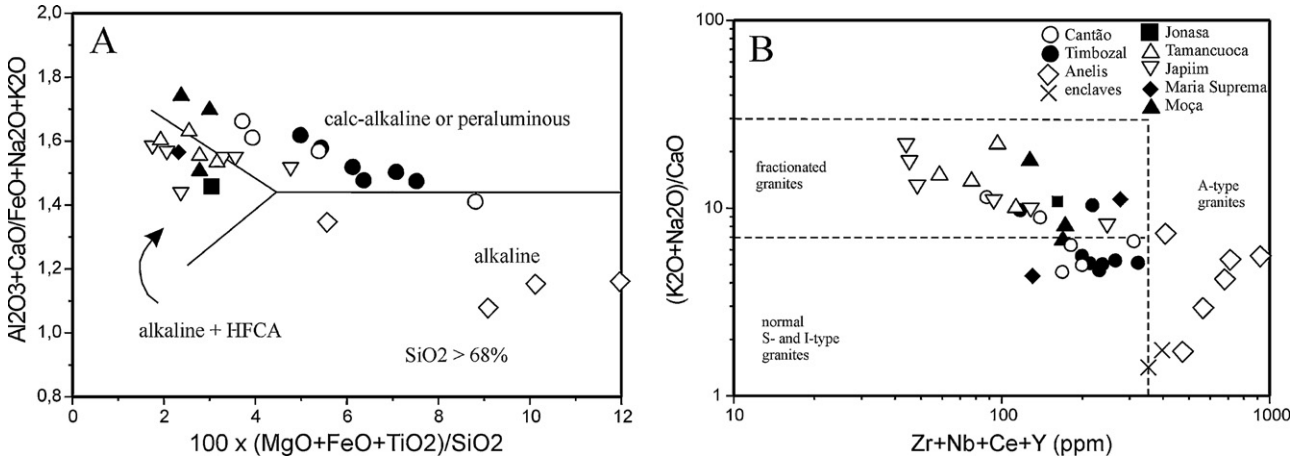

Fig. 13. Discriminant of granitoid types of (A) Sylvester (1998) and (B) Whalen et al. (1987). HFCA: highly fractionated calc-alkaline.

Strongly peraluminous rocks are in general associated with large-scale shear and thrust zones and with subduction and syn- to post-collision processes along orogenic belts. These environments channel considerable amounts of water favoring the production of muscovite- and biotite-bearing peraluminous magmas. Furthermore, strongly peraluminous granites are products of reworking (melting) of ancient crust and its detrital products mixed or not with mantle-derived products (Pearce et al., 1984; Barbarin, 1996, 1999; Sylvester, 1998; Collins and Richards, 2008; Bagas et al., 2010). Moreover, petrogenetic modeling studies indicate that the genesis and the causes of chemical variation within granitic rock series in general, including leucogranites and S-type granites, stem from inheritance of the magma sources (Villaros et al., 2009; Clemens and Stevens, 2012, and references therein).

Some examples, however, indicate that strongly peraluminous may not be necessarily associated with collision. According to Collins and Richards (2008), the S-type granites may also form in response to backarc extension. Furthermore, overlapping of I- and S-type magmatism in space and time may be associated to the change of regional compression to extension at the final stages of accretionary orogenesis occurring in a convergent plate margin (Cawood et al., 2011).

The absence of associated high-grade rocks and the local presence of granitic mobilized within gneisses (local migmatization of the Itapeva Complex, Klein et al., 2005b), suggest that the muscovite-bearing granites and leucogranites have been produced by anatexis and that magma ascent occurred probably in crustal scale shear zones (e.g., Brown, 1994). The high and restricted SiO_2 contents, the low MgO concentrations, and the presence of primary muscovite and, in places, pegmatites, indicate that the peraluminous granites formed by partial melting of crustal materials in a volatile-rich system (when pegmatites are present), or formation from highly evolved magmas. Furthermore, in our study, some lines of evidence indicate that the parental magmas for the strongly peraluminous muscovite-bearing granites and leucogranites comprise mixtures of different proportions of melts derived from aluminous crustal materials (pelitic and psammitic sediments), greywackes and, in general, subordinate basaltic melts or mantle derived components (except Maria Suprema, that appears to have a predominant contribution from basaltic magmas). The evidence include: (1) except for the Japiim Granite that shows a syn-collision signature, all other granites have volcanic arc signature (Fig. 15), (2) the Rb/Sr versus Rb/Ba (Fig. 14A) and Al_2O_3/TiO_2 versus CaO/Na_2O relationships (Fig. 14A), (3) the moderate to high $Al_2O_3/(FeO^* + MgO + TiO_2)$ ratios (Fig. 14B), (4) the Nd isotope signature (Fig. 12), (5) the age spectra of the inherited zircon populations, and (6) the absence of magmatic enclaves and xenoliths of metasedimentary rocks.

Archean sedimentary sources are not known in the region so far, and Archean ages, in general, are very limited in the Gurupi Belt, as discussed in the previous section. Mafic igneous rocks and psammites/greywackes appear to be the dominant sources for the

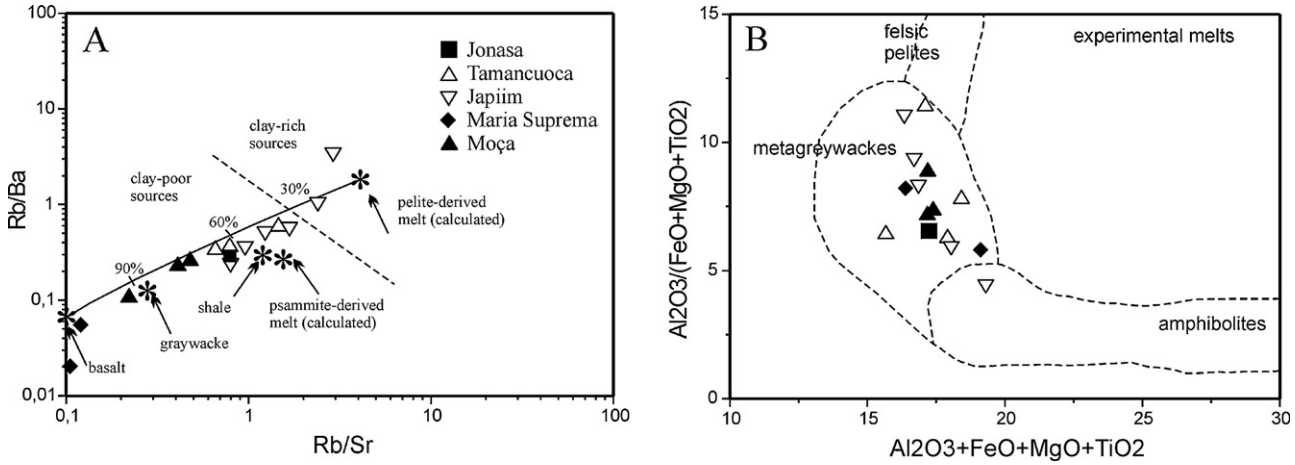

Fig. 14. Trace and major element diagrams that investigate possible sources for peraluminous granites. (A) Rb/Sr versus Rb/Ba diagram of Sylvester (1998); (B) $Al_2O_3 + Fe_2O_3 + MgO + TiO_2$ versus $Al_2O_3/(Fe_2O_3 + MgO + TiO_2)$ diagram of Patiño Douce (1999).

Moça and Maria Suprema magmas (Fig. 14). However, the absence of mafic and restitic enclaves in these leucogranites is not in keeping with a major role played by basic magmas. Furthermore, the known greywackes belong to the Gurupi Group and are quite younger than the muscovite-bearing granites. A better alternative for basaltic sources are the juvenile rocks of the São Luís cratonic fragment (Tromaí Intrusive Suite) and basement of the Gurupi Belt (Itapeva Complex) of 2167–2140 Ma, which are composed mostly of granodiorite and tonalite. Melting of biotite-rich felsic to intermediate rocks in middle- to lower-crust conditions is a possible source for peraluminous magmas (Bagas et al., 2010). In fact, field relationships are consistent with local melting and in situ migmatization of biotite-gneisses of the Itapeva Complex (Klein et al., 2005b; Klein and Lopes, 2011). These juvenile units might also be, at least in part, responsible for the "greywacke" signature, since the average composition of greywackes is intermediate between the compositions of granodiorite and tonalite (e.g., Condie, 1981). It is also possible that the magmas that produced the true leucogranites (mafic minerals <5%, i.e., Tamancuoca and Japiim types) represent pure melts from the anatectic source. Therefore, mixing of variable proportions of distinct classes of source materials were responsible for the variation observed among different bodies of the peraluminous granites and further petrogenetic modeling is needed to infer better the more probable sources for each of the muscovite-bearing granites.

7.6. Origin of the potassic granitoids

The potassic granitoid units represent two or three (depending on the use of the analytical errors of the U–Pb data) different stages of magmatism occurring at about 2.16 Ga (Cantão Granodiorite), 2.10 Ga (Anelis Intrusive Suite), and 2.08 Ga (Timbozal Monzogranite). Cantão is a high-K, calc-alkaline, I-type pluton and, despite having the same age of the juvenile Tromaí Intrusive Suite, it do not belong to this magmatic suite, as demonstrated by its geochemical and Nd signature, all indicating crustal (± mantle) derivation for this unit.

The Anelis Intrusive Suite is an alkalic association, in the sense of Frost et al. (2001). The suite is highly enriched in K_2O and Na_2O and shows high Ba–Rb–Sr and Zr–Ce–Th–Y contents and high Th/Yb ratios. As a whole, the suite has complex chemical characteristics that are compatible with those of the shoshonitic series, A-type, volcanic arc and late-orogenic granites (Figs. 13 and 15).

The Timbozal Monzogranite is a high-K calc-alkaline pluton, with geochemical characteristics very similar to those of the Cantão Granodiorite, despite the age difference. The entrainment of crustal materials to the magma is supported by the presence of xenoliths of supracrustal calc-silicate rocks and of granitoids in the Timbozal Monzogranite. It is noteworthy that the enclaves of quartz syenite and monzogranite are compositionally similar to the Anelis Intrusive Suite rocks. This indicates that the Anelis rocks might be part of the source of the Timbozal rocks or that Anelis is the host rock for the emplacement of the Timbozal Monzogranite.

The three K-rich suites show, in general, chemical and isotopic characteristics that are consistent with both arc (juvenile) and crust sources. The negative Ba, Nb, Ta, P and Ti negative anomalies might be produced by fractional crystallization and/or be inherited from a previous subduction. Alone, the coupled negative Nb–Ta anomalies indicate that the rocks have been produced by chemical differentiation of arc-derived magmas. This might be, nevertheless, also an inheritance. Crust participation is indicated by the presence of enclaves of igneous, metamorphic and sedimentary rocks, and the positive U and Pb anomalies relative to primitive mantle values (figures not included) that suggest that the magmas derive from, or interacted with, upper crustal materials.

7.7. Timing and tectonic setting of the Rhyacian magmatism in the basement of the Gurupi Belt

The studied granitoids do not occur as a continuous continental block, but as isolated bodies within younger metasedimentary successions. This fact brings additional difficulties in the interpretation of the tectonic setting in which they have formed and of possible sources for the magmas. Notwithstanding, the granitoids occur in relatively close spatial relationship and an attempt is made to infer this setting. Geochronology shows that potassic-alkalic granitoids formed at least in two periods (analytical errors included), 2159–2167 Ma (Cantão), and 2079–2121 Ma (Anelis, Timbozal) and that peraluminous granites formed at 2133–2151 Ma (Jonasa) and 2072–2130 Ma (Moça, Japiim, Tamancuoca, Maria Suprema).

In tectonic discriminant diagrams the potassic-alkalic granitoids show chemical characteristics compatible with those of volcanic arc, syn-collision and late orogenic granites (Fig. 15). In the same diagrams, the two-mica granites show both collision and volcanic arc characteristics, depending on the element relationships, and only the Japiim type consistently shows syn-collision signature. However, the arc signature likely reflects the sources of the magmas instead of the tectonic setting in which the granites formed. Sylvester (1998) states that the strongly peraluminous granites are post-collision rocks because their emplacement occurs after the crustal thickening and that may be syn- or post-tectonic granites depending on their relationships with shear zones and deformation. In the Gurupi Belt all rocks show some degree of deformation, but only the Tamancuoca and Maria Suprema granites are strongly deformed. It is uncertain, however, whether this deformation is related to the Rhyacian or Neoproterozoic-Early Cambrian events, although Klein et al. (2005b) stated that deformation of the Maria Suprema Granite was coeval to its intrusion into the gneisses of Itapeva Complex. Also according to Sylvester (1998), the predominance of pelitic sedimentary sources indicates mature and deeply eroded continental platforms, whereas the predominance of psammitic sources suggests immature plate margin, such as island arc and continental arc associations. The strongly peraluminous granitoids addressed in this study, show predominantly characteristics of clay-poor, psammitic-rich sources.

Integrating field, petrographic, geochemical, geochronological and Nd isotope information, crustal sources and active continental margin – collision settings are inferred for the different types of basement granitoids of the Gurupi Belt. We are aware, however, that the hypothesis of a collisional event must be further developed.

8. Regional and global correlations

In previous works, the interpreted orogenic evolution of the São Luís cratonic fragment in the Paleoproterozoic Era involved the following stages (Fig. 16): (1) <2260 Ma – opening of an oceanic basin; (2) 2240–2210 Ma – early island arc and associated basins; (3) 2167–2150 Ma – intra-oceanic arc construction associated with transitional/continental arc development; (4) ~2100 Ma – collision and (5) ~2050–2070 Ma – late- to post-orogenic/collision potassic magmatism. Stage "4" has been considered to be better represented in the basement of the Gurupi Belt (Klein et al., 2005b, 2008, 2009; Palheta et al., 2009). As such, the understanding is that the rock units of the present day São Luís cratonic fragment and of the basement of the Gurupi Belt formed a single crustal block in the Paleoproterozoic Era. Those units that have not been affected by the Neoproterozoic-Early Cambrian events that built up the Gurupi Belt became what is now known as São Luís cratonic fragment. The results of our study bring additional constraints on the previously outlined evolution. The Rhyacian rock units addressed in this study may be associated in time and type of magmatism with stages "3"

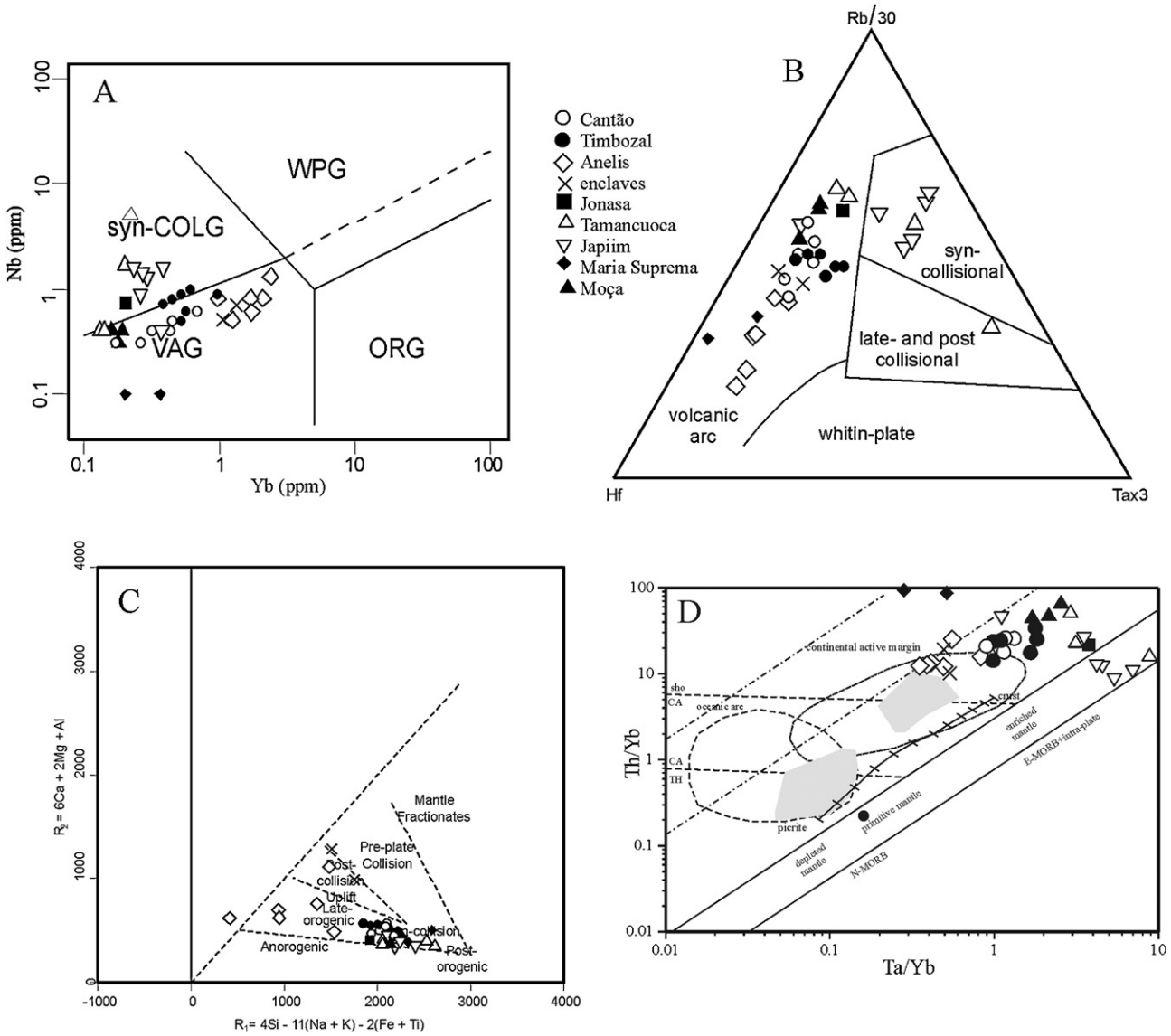

Fig. 15. Tectonic discriminant diagrams. (A) Yb × Nb plot of Pearce et al. (1984); (B) Hf–Rb–Ta ternary diagram of Harris et al. (1986); (C) R1-R2 cationic plot of Batchelor and Bowden (1985); (D) Ta/Yb × Th/Yb plot combining the fields proposed by Pearce (1982) (heavy and dashed lines) and those from Gorton and Schandl (2000) (dotted lines). The graduated line picrite-crust indicates theoretical mixing lines between primitive mantle and upper crust (as calculated by Bagas et al., 2010) and the gray areas represent the composition of the juvenile, arc-related Tromaí Intrusive Suite (as defined by Klein et al., 2008).

(Cantão Granodiorite – continental arc), "4" (the strongly peraluminous granites – collision), and "5" (the potassic Timbozal and Anelis granitoids – post collision). The role of the Jonasa Granodiorite remains poorly understood, however, considering its age, it is probably associated to the continental arc phase (Fig. 16).

In the eastern portion of the Guiana Shield of the Amazonian Craton (Fig. 1B), i.e., State of Amapá in Brazil and French Guyana, there are rock associations formed approximately in the same periods than those described for the São Luís-Gurupi region. Gneisses and calc-alkaline granitoids that formed between 2190 and 2140 Ma intruded older (>2260 Ma) metavolcano-sedimentary rocks, and are associated to coeval metavolcano-sedimentary rocks, resembling the Aurizona-Tromaí-Chega Tudo association of the São Luís-Gurupi region. These associations have been interpreted as formed in magmatic arc setting (Delor et al., 2003; Rosa-Costa et al., 2006 and references therein). A significant difference resides in the juvenile characteristics of the São Luís rocks. Syn- to post-collisional granitoids, including peraluminous types, formed between 2100 and 2030 Ma in the Guyana Shield, and are associated with coeval high-grade metamorphism. Metamorphism in the Gurupi Belt is limited to the amphibolite facies conditions. All these associations have been related to the Trans-Amazonian cycle (Delor et al., 2003; Santos et al., 2003; Rosa-Costa et al., 2006 and references therein).

Regarding this cycle, the term Trans-Amazonian is widely and loosely used in South America to refer to orogenic cycle, orogenic event, orogeny or even rock ages. In a classical work, based on Rb–Sr and K–Ar ages, Hurley et al. (1967) defined the Trans-Amazonian Orogenic Cycle, which is obviously the more appropriate term, considering that a cycle may contain several orogenies developing at the same time, or in different portions of the crust and even diachronically. Almeida et al. (1973) framed the temporal limits of the cycle between 2200 and 1800 Ma and, more recently, and using a U–Pb dataset, Santos et al. (2003) refined these limits for the 2264–2011 Ma range, and extended the influence or occurrence of the cycle to the entire South American continent. Furthermore, as discussed in Klein et al. (2008), Santos et al. (2003) considered the São Luís cratonic fragment as the type-area of the Trans-Amazon orogen, based on data published in Klein and Moura (2001 and

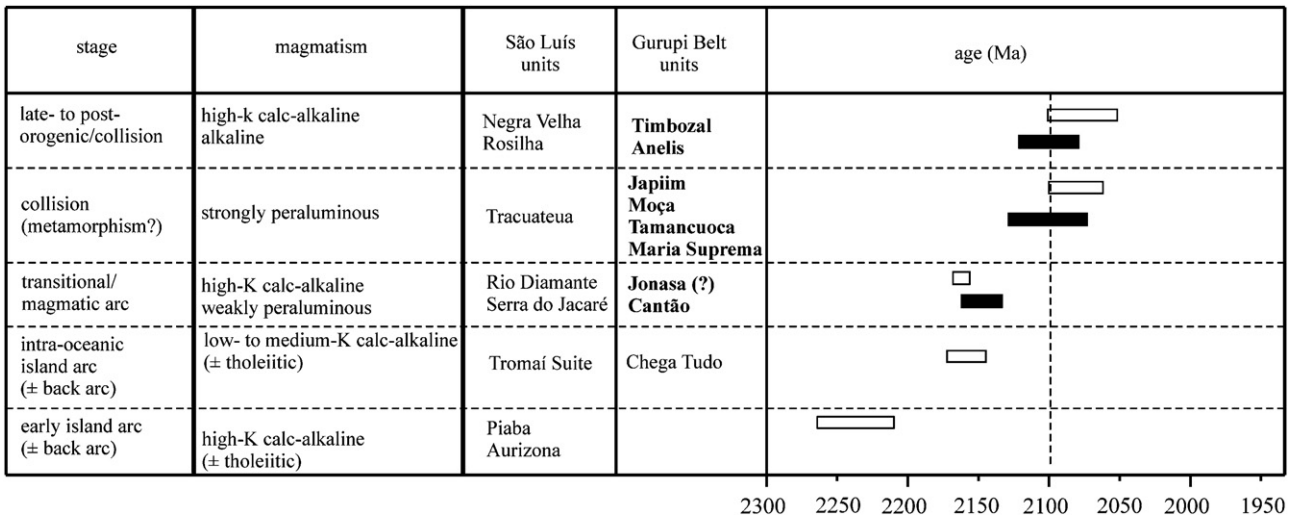

Fig. 16. Summary of crystallization ages for the magmatic events recognized in the São Luís Cratonic Fragment (white bars) and basement of the Gurupi Belt (black bars). Rock units in bold characters are those addressed in this study. The vertical dashed line indicates the inferred timing for the Rhyacian metamorphism.

references therein). Moreover, Santos et al. (2003) defined four orogenies in this supposed type-area. To Brito Neves (2007) the use of "Trans-Amazonian" should be restricted to the Amazonian Craton, but would also be permissive of usage up in West Africa.

Combining the data from the São Luís cratonic fragment and the diverse granitoid units from the basement of the Gurupi Belt, we envisage a protracted accretionary orogenic cycle involving different settings (island arc, back-arc, sedimentary basin, continental margin – Klein et al., 2008, 2009, and this work) that have eventually been involved in a collision phase (e.g., Cawood et al., 2009) against a continental block which could be represented, at least in part, by the Archean Igarapé Grande Metatonalite (Fig. 1C). We do not have elements to interpret this scenario as a sequence of four orogenies as proposed by Santos et al. (2003). Furthermore, although we do not discard the interpretation of Santos et al. (2003) as a working hypothesis, and following Klein et al. (2008), we understand that the scenario described above displays similarities with juvenile portions of the Rhyacian (Eburnean-Birimian) terranes of the Baoulé-Mossi domain of the West African Craton, in terms of rock associations, tectonic setting and age of magmatic events. As a consequence, São Luís and the Rhyacian basement of the Gurupi Belt are more likely a fragment (or fragments) of the West African Craton (Hurley et al., 1967; Klein and Moura, 2008 and references therein). This landmass remained relatively stable until its incorporation into the Rodinia supercontinent and subsequently participated of the assembly of West Gondwana and that, eventually, remained in South America after the breakup of Pangea (Hurley et al., 1967; Condie, 2002; Klein and Moura, 2008 and references therein).

9. Concluding remarks

Previous works have revealed that the Paleoproterozoic evolution of geological units from the basement of the Gurupi Belt comprise calc-alkaline rocks of 2160–2147 Ma and peraluminous granites of about 2100 Ma. These associations and periods are consistent with the accretionary (2240–2150 Ma) and the collisional (ca. 2100 Ma) phases, respectively, described for the neighboring São Luís cratonic fragment. In this work we have brought more precision to the timing of what we redefined as strongly peraluminous magmatism and also identified potassic-alkalic and an older (weakly) peraluminous event. Field (structural, limited cross-cutting relationships) and petrographic characteristics, geochronology, and geochemical and isotopic data of the granitoids of the basement of the Neoproterozoic-Early Cambrian Gurupi Belt indicate contrasting aspects and record five stages and/or types of plutonic activity during the Rhyacian period. The stages and granitoid types are:

(1) 2163 Ma-old, weakly peraluminous, high-K_2O, crust-derived and weakly deformed granodiorite to granite, represented by the Cantão Granodiorite; this event is coeval with the main phase of subduction-related, juvenile, calc-alkaline granitoid magmatism of the São Luís cratonic fragment (Tromaí Intrusive Suite) and with that detected in protoliths of some gneisses from the basement of the southeastern portion of the Gurupi Belt (Itapeva Complex).
(2) 2142 Ma-old, weakly peraluminous, biotite- and muscovite-bearing granodiorites of crustal origin of the Jonasa Granodiorite that underwent metamorphism and strong deformation at ca. 525 Ma; this unit is slightly younger and compositionally distinct from the Tromaí Intrusive Suite and from the Cantão Granodiorite.
(3) 2116–2079 Ma-old, crust-derived, strongly peraluminous, biotite- and muscovite-bearing granites and leucogranites possibly formed in a collisional setting belonging to the Japiim, Tamancuoca, Moça and Maria Suprema granites.
(4) 2100 Ma-old, metaluminous to slightly peralkaline, potassic granites to quartz-syenites, spatially associated with the peraluminous magmatism, and represented by the Anelis Intrusive Suite;
(5) 2085 Ma-old, weakly peraluminous, high-K_2O, crust-derived granite, represented by the Timbozal Monzogranite that intruded the Anelis Suite.

The intrusion of the strongly peraluminous granites and of the different generations of potassic/alkalic granitoids is interpreted to have occurred in a transitional environment from syn-collision (compressional) to late/post-collision (extensional) event that resulted from crustal thickening caused by active continental margin subduction and arc-continent collision occurring around 2100 Ma in the southwestern portion of the São Luís-West African Craton. This continent is still unknown and might be concealed under the Phanerozoic cover as suggested by Klein et al. (2005b) or might be partially represented by the Archean Igarapé Grande Metatonalite that make also part of the basement of the Gurupi Belt.

The Cantão Granodiorite likely represents a remnant of the continental arc, whereas the peraluminous granites define the (syn- to post-) collisional stage and the Anelis and Timbozal units are associated with the latest, post-orogenic/collision events. The weakly peraluminous event at 2143 Ma is not yet fully understood and a more robust chemical and geochemical dataset is required to resolve this. The studied granitoid types also show evidence of variable inherited ages that indicate Archean to Paleoproterozoic sources involved in magma genesis.

Acknowledgments

The paper is a contribution of CPRM-Geological Survey of Brazil through the Gurupi Project. Hilton T. Costi (Museu Paraense Emílio Goeldi) and Claudio N. Lamarão (UFPA) are thanked for helping with zircon imaging. The senior author acknowledges the Brazilian Conselho de Desenvolvimento Científico e Tecnológico (CNPq) for a research grant (306723/2009-3). We thank Dr. João Orestes Schneider dos Santos, an anonymous reviewer, and Dr. Peter Cawood for critical comments on the manuscript.

Appendix A. Summary of analytical procedures

U–Pb LA-ICP-MS analyses were undertaken at the Laboratório de estudos geocronológicos, geodinâmicos e ambientais of the Universidade de Brasília (UNB), Brasília, Brazil, and one sample was analyzed in the Laboratório de Geologia Isotópica of the Universidade Federal do Rio Grande do Sul, in Porto Alegre, Brazil. In both laboratories the analyses followed procedures described in detail in Bühn et al. (2009). Concentrates of zircon were obtained by crushing the rock and then sieving, panning and using a magnetic separator and dense liquid (bromoform). Zircon crystals were hand-picked under a binocular microscope, mounted in epoxy resin, and polished with diamond paste; carbon-coating was applied before imaging and a conductive gold-coating was applied just prior to isotopic analysis. The analyses were performed with a Thermo Finnigan Neptune multicollector inductively coupled plasma mass spectrometer with an attached New Wave 213 μm Nd-YAG solid state laser. The acquisition followed a standard – sample bracketing technique with four sample analyses between a blank and a GJ-1 zircon standard. Ablation was done with a spot size of 25–30 μm. The accuracy was controlled using the standard TEMORA-2 or UQZ. Raw data were reduced using an in-house program and corrections were done for background, instrumental mass-bias drift and common Pb, as described in Bühn et al. (2009). The ages were calculated using ISOPLOT 3.0 (Ludwig, 2003). Analyses for individual spots are plotted on concordia diagrams with 1σ uncertainties. Where data are combined to calculate an age, the quoted uncertainties are at 95% confidence level, with uncertainties in the U–Pb standard calibration included in any relevant U–Pb intercept and concordia age calculations. Analyses were preceded by cathodoluminescence and/or Backscattered Electron imagery done at the Universidade Federal do Pará and Museu Paraense Emilio Goeldi, respectively, in Belém, Brazil.

Sm–Nd analyses were also undertaken at the UNB laboratory and the analytical procedures for Sm–Nd analyses are described in Gioia and Pimentel (2000). Fifty mg of whole rock powders were mixed with a $^{149}Sm/^{150}Nd$ spike and dissolved in Savilex vessels. The Sm–Nd separation used cation exchange Teflon columns with Ln-Spec resin, then Sm and Nd were deposited in Re filaments and the isotopic ratios were determined on a FINNIGAN MAT 262 mass spectrometer using the static mode. The Nd data were normalized to a $^{146}Nd/^{144}Nd$ ratio of 0.7219 and uncertainties in the Sm/Nd and $^{143}Nd/^{144}Nd$ ratios were about 0.4% (1σ) and 0.005% (1σ), respectively, based on repeated analysis of the BHVO-1 and BCR-1 standards. The crustal residence ages were calculated using the values of DePaolo (1981) for the depleted mantle (T_{DM}).

Major and trace elements were determined by ICP-ES and ICP-MS, respectively, at Acme Analytical Laboratories Ltd. in Canada, and after Li metaborate/tetraborate fusion. Chemical diagrams were partly produced using the GCDkit software (Janousek et al., 2003).

Appendix B. Supplementary data

Supplementary data associated with this article can be found, in the online version, at http://dx.doi.org/10.1016/j.precamres.2012.08.007.

References

Abreu, F.A.M., Lesquer, A., 1985. Considerações sobre o Pré-Cambriano da região sul-sudoeste do Cráton São Luís. In: Simpósio de Geologia da Amazônia, 2, Belém. Anais.. SBG, vol. 1, pp. 7–21.
Almeida, F.F.M., Amaral, G., Cordani, U.G., Kawashita, K., 1973. The Precambrian evolution of the South American cratonic margin south of the Amazon river. In: Nairn, A.E.M., Stehli, F.G. (Eds.), The Ocean Basins and Margins, vol. 1. Plenum Pub. Corp., pp. 411–446.
Almeida, F.F.M., Hasui, Y., Brito Neves, B.B., 1976. The Upper Precambrian of South América. Boletim Instituto de Geociências USP 7, 45–80.
Bagas, L., Bierlein, F.P., Anderson, J.A.C., Maas, R., 2010. Collision-related granitic magmatism in the Granites-Tanami Orogen, Western Australia. Precambrian Research 177, 212–226.
Barbarin, B., 1996. Genesis of the two main types of peraluminous granitoids. Geology 24, 295–298.
Barbarin, B., 1999. A review of the relationships between granitoid types, their origins and their geodynamic environments. Lithos 46, 605–626.
Batchelor, R.A., Bowden, P., 1985. Petrogenetic interpretation of granitic rock series using multicationic parameters. Chemical Geology 48, 43–55.
Borges, M.S., Angélica, R.S., Costa, M.L., 1988. Contribuição à geologia da região de Santa Luzia do Pará, nordeste do Pará. In: SBG, Congresso Brasileiro de Geologia 35. Anais, vol. 6, pp. 2689–2703.
Boynton, W.V., 1984. Cosmochemistry of the rare-earth elements: meteorite studies. In: Henderson, P. (Ed.), Rare-Earth Elements Geochemistry. Amsterdam, Elsevier, pp. 63–114.
Brito Neves, B.B., 2007. O Ciclo Transamazônico sob questionamento. In: Simpósio Brasileiro de Estudos Tectônicos, 11. Natal, Sociedade Brasileira de Geologia, Abstracts, pp. 119–121.
Brito Neves, B.B., Fuck, R.A., Cordani, U.G., Thomaz Filho, A., 1984. Influence of basement structures on the evolution of the major sedimentary basins of Brazil: a case of tectonic heritage. Journal of Geodynamics 1, 495–510.
Brown, M., 1994. The generation, segregation, ascent and emplacement of granite magma: the migmatite-to-crustally-derived granite connection in thickened orogens. Earth-Science Reviews 36, 83–130.
Bühn, B., Pimentel, M.M., Matteini, M., Dantas, E.L., 2009. High spatial resolution analysis of Pb and U isotopes for geochronology by laser ablation multi-collector inductively coupled plasma mass spectrometry (LA-MC-IC-MS). Anais da Academia Brasileira de Ciências 81, 1–16.
Cawood, P.A., Kröner, A., Collins, W.J., Kusky, T.M., Mooney, W.D., Windley, B.F., 2009. Accretionary orogens through Earth history. In: Cawood, P.A., Kröner, A. (Eds.), Earth Accretionary Systems in Space and Time. Geological Society, London, Special Publications 318, 1–36.
Cawood, P.A., Leitch, E.C., Merle, R., Nemchin, A.A., 2011. Orogenesis without collision: stabilizing the Terra Australis accretionary orogen, eastern Australia. Geological Society of America Bulletin 123, 2240–2255.
Clemens, J.D., Stevens, G., 2012. What controls chemical variation in granitic magmas. Lithos 134–135, 317–329.
Collins, W.J., Richards, S.W., 2008. Geodynamic significance of S-type granites in circum-Pacific orogens. Geology 36, 559–562.
Condie, K.C., 1981. Archean Greenstone Belts. Elsevier, Amsterdam.
Condie, K.C., 2002. Breakup of a Paleoproterozoic supercontinent. Gondwana Research 5, 41–43.
Cordani, U.G., Brito Neves, B.B., Fuck, R.A., Porto, R., Thomaz Filho, A., Cunha, F.M.B., 1984. Estudo preliminar de integração do Pré-Cambriano com os eventos tectônicos das bacias sedimentares brasileiras. PETROBRAS, Rio de Janeiro, 70 pp. (Série Ciências-Técnicas-Petróleo, Seção: Exploração de Petróleo, 15).
Corfu, F., Hanchar, J.M., Hoskin, P.W.O., Kinny, P., 2003. Atlas of zircon textures. In: Hanchar, J.M., Hoskin, P.W.O. (Eds.), Zircon. Reviews in Mineralogy and Geochemistry, Mineralogical Society of America/Geochemical Society 53, 469–500 (Chapter 16).
Costa, J.L., 2000. Programa Levantamentos Geológicos Básicos do Brasil. Programa Grande Carajás. Castanhal, Folha SA.23-V-C. CPRM, Estado do Pará, Belém (CD-ROM).
Costa, J.L., Almeida, H.G.G., Ricci, P.S.F., 1996. Metamorfismo e divisão tectono-estratigráfica do Grupo Gurupi no nordeste do Pará e noroeste do Maranhão. In:

Simpósio de Geologia da Amazônia, 5, Belém, Boletim de resumos expandidos, SBG, pp. 110–112.
Delor, C., Egal, E., Lafon, J.M., Cocherie, A., Guerrot, C., Rossi, P., Truffert, C., Théveniaut, H., Phillips, D., Avelar, V.G., 2003. Transamazonian crustal growth and reworking as revealed by the 1:500,000-scale geological map of French Guiana (2nd edition). Géologie de la France 2-3-4, 5–57.
De Kock, G.S., Armstrong, R.A., Siegfried, H.P., Thomas, E., 2011. Geochronology of the Birim Supergroup of the West African craton in the Wa-Bolé region of central-west Ghana: implications for the stratigraphic framework. Journal of African Earth Sciences 59, 1–40.
DePaolo, D.J., 1981. A neodymium and strontium isotopic study of the Mesozoic calc-alkaline granitic batholiths of the Sierra Nevada and Peninsular Ranges, California. Journal of Geophysical Research 86, 10470–10488.
Drummond, M.S., Defant, M.J., 1990. A model for trondhjemite–tonalite–dacite genesis and crustal growth via slab melting: Archean to modern comparisons. Journal of Geophysical Research 95, 21503–21521.
Dostal, J., Chatterjee, A.K., 2000. Contrasting behavior of Nb/Ta and Zr/Hf ratios in a peraluminous granitic pluton (Nova Scotia, Canada). Chemical Geology 163, 207–218.
Faure, G., 1986. Principles of Isotope Geology, 2nd ed. John Wiley & Sons, New York, 589 pp.
Foley, S.F., Wheller, G.E., 1990. Parallels in the origin of the geochemical signatures of island arc volcanics and continental potassic igneous rocks: the role of residual titanites. Chemical Geology 85, 1–18.
Frost, B.R., Barnes, C.G., Collins, W.J., Ellis, D.J., Frost, C.D., 2001. A geochemical classification for granitic rocks. Journal of Petrology 42, 2033–2048.
Geisler, T., Ulonska, M., Schleicher, H., Pidgeon, R.T., van Bronswijk, W., 2001. Leaching and differential recrystallization of metamict zircon under experimental hydrothermal conditions. Contributions to Mineralogy and Petrology 141, 53–65.
Gioia, S.M.L.C., Pimentel, M.M., 2000. The Sm–Nd method in the geochronology laboratory of the University of Brasília. Anais da Academia Brasileira de Ciências 72, 219–245.
Gorton, M.P., Schandl, E.S., 2000. From continents to island arcs: a geochemical index of tectonic setting for arc-related and within-plate felsic to intermediate volcanic rocks. The Canadian Mineralogist 38, 1065–1073.
Harley, S.L., Kelly, N.M., Möller, A., 2007. Zircon behavior and the thermal histories of mountain chains. Elements 3, 25–30.
Harris, N.B.W., Pearce, J.A., Tindle, A.G., 1986. Geochemical characteristics of collision-zone magmatism. In: Coward, M.P., Ries, A.C. (Eds.), Collision Tectonics. Geological Society, London, Special Publications 19, 67–81.
Hasui, Y., Abreu, F.A.M., Villas, R.N.N., 1984. Província Parnaíba. In: Almeida, F.F.M., Hasui, Y. (Eds.), O Pré-Cambriano no Brasil. Edgard Blücher, São Paulo, pp. 36–45.
Hoskin, P.W.O., Schaltegger, U., 2003. The composition of zircon and igneous and metamorphic petrogenesis. In: Hanchar, J.M., Hoskin, P.W.O. (Eds.), Zircon. Reviews in Mineralogy and Geochemistry 53, 27–62.
Hurley, P.M., Almeida, F.F.M., Melcher, G.C., Cordani, U.G., Rand, J.R., Kawashita, K., Vandoros, P., Pinson, W.H., Fairbairn, H.W., 1967. Test of continental drift by comparison of radiometric ages. Science 157, 495–500.
Jahn, B.M., Liu, D., Wan, Y., Song, B., Wu, J., 2008. Archean crustal evolution of the Jiaodong peninsula, China, as revealed by zircon SHRIMP geochronology, elemental and Nd-isotope geochemistry. American Journal of Science 308, 232–269.
Janousek, V., Farrow, C.M., Erban, V., 2003. GCDkit: new PC software for interpretation of whole-rock geochemical data from igneous rocks. Godschmidt Conference Abstracts, A186.
Jochum, K.P., Stolz, A.J., McOrist, G., 2000. Niobium and tantalum in carbonaceous chondrites: constraints on the solar system and primitive mantle niobium/tantalum, zirconium/niobium, and niobium/uranium ratios. Meteorite and Planetary Science 35, 229–235.
Klein, E.L., Lopes, E.C.S., 2009. Formação Igarapé de Areia: Tarkwa no Cinturão Gurupi? In: II Simpósio Brasileiro de Metalogenia, Gramado, Abstracts, (CD-ROM).
Klein, E.L., Lopes, E.C.S., 2011. Geologia e recursos minerais da Folha Centro Novo do Maranhão – SA.23-Y-B-I, Estados do Maranhão e Pará, Escala 1:100.000. CPRM, Belém (CD-ROM).
Klein, E.L., Lopes E.C.S. Geologia e recursos minerais da Folha Santa Luzia do Pará – SA.23-V-C-VI, Estado do Pará, Escala 1:1.000.000. CPRM-Geological Survey of Brazil, Belém, in press.
Klein, E.L., Moura, C.A.V., 2001. Age constraints on granitoids and metavolcanic rocks of the São Luís craton and Gurupi belt, northern Brazil: implications for lithostratigraphy and geological evolution. International Geology Review 43, 237–253.
Klein, E.L., Moura, C.A.V., 2003. Sintese geológica e geocronológica do Craton São Luís e do Cinturão Gurupi na região do rio Gurupi (NE-Para/NW-Maranhão). Revista Geologia USP, Série Científica 3, 97–112.
Klein, E.L., Moura, C.A.V., 2008. São Luís craton and Gurupi belt (Brazil): possible links with the West-African craton and surrounding Pan-African belts. In: Pankhurst, R.J., Trouw, R.A.J., Brito Neves, B.B., de Wit, M.J. (Eds.), West Gondwana: Pre-Cenozoic Correlations Across the South Atlantic Region. Geological Society, London, Special Publications 294, 137–151.
Klein, E.L., Moura, C.A.V., Pinheiro, B.L.S., 2005a. Paleoproterozoic crustal evolution of the São Luís Craton, Brazil: evidence from zircon geochronology and Sm–Nd isotopes. Gondwana Research 8, 177–186.
Klein, E.L., Moura, C.A.V., Krymsky, R., Griffin, W.L., 2005b. The Gurupi belt in northern Brazil: lithostratigraphy, geochronology, and geodynamic evolution. Precambrian Research 141, 83–105.
Klein, E.L., Luzardo, R., Moura, C.A.V., Armstrong, R., 2008. Geochemistry and zircon geochronology of paleoproterozoic granitoids: further evidence on the magmatic and crustal evolution of the São Luís cratonic fragment, Brazil. Precambrian Research 165, 221–242.
Klein, E.L., Luzardo, R., Moura, C.A.V., Lobato, D.C., Brito, R.S.C., Armstrong, R., 2009. Geochronology, Nd isotopes and reconnaissance geochemistry of volcanic and metavolcanic rocks of the São Luís Craton, northern Brazil: implications for tectonic setting and crustal evolution. Journal of South American Earth Sciences 27, 129–145.
Kober, B., 1986. Whole grain evaporation for $^{207}Pb/^{206}Pb$ age investigations on single zircons using a double filament source. Contributions to Mineralogy and Petrology 93, 482–490.
Lesquer, A., Beltrão, J.F., Abreu, F.A.M., 1984. Proterozoic links between northeastern Brazil and West Africa: a plate tectonic model based on gravity data. Tectonophysics 110, 9–26.
Lowell, G.R., Villas, R.N.N., 1983. Petrology of nepheline syenite gneiss from Amazonian Brazil. Geological Journal 18, 53–75.
Lucas, F.R.A., Moura, C.A.V., Klein, E.L., 2009. Geologia e idade $^{207}Pb/^{206}Pb$ em zircão detrítico em conglomerados da região do Gurupi, nordeste do Pará. In: Simpósio de Geologia da Amazônia, 11, SBG, Resumos, (CD-ROM).
Ludwig, K.R., 2003. Isoplot 3.00 – A Geochronological Toolkit for Microsoft Excel. Berkeley Geochronology Center, Special Publication, 4.
Münker, C., 1998. Nb/Ta fractionation in a Cambrian arc/back arc system, New Zealand: source constraints and application of refined ICPMS techniques. Chemical Geology 144, 23–45.
Palheta, E.S., Abreu, F.A.M., Moura, C.A.V., 2009. Granitóides proterozóicos como marcadores da evolução geotectônica da região nordeste do Pará – Brasil. Revista Brasileira de Geociências 39, 647–657.
Pastana, J.M.N., 1995. Programa Levantamentos Geológicos Básicos do Brasil. Programa Grande Carajás. Turiaçu/Pinheiro, folhas SA.23-V-D/SA.23-Y-B. CPRM, Estados do Pará e Maranhão, Brasília, 205 pp.
Patiño Douce, A.E., 1999. What do experiments tell us about the relative contributions of crust and mantle to the origin of granitic magmas? Geological Society, London, Special Publications 168, 55–75.
Pearce, J.A., 1982. Trace element characteristics of lavas from destructive plate boundaries. In: Thorpe, R.S. (Ed.), Andesites. Wiley, New York, pp. 525–528.
Pearce, J.A., Harris, N.B.W., Tindle, A.G., 1984. Trace element discrimination diagrams for the tectonic interpretation of granitic rocks. Journal of Petrology 25, 956–983.
Peccerilo, A., Taylor, S.R., 1976. Geochemistry of Eocene calc-alkaline volcanic rocks from the Kastamonu area, northern Turkey. Journal of Petrology 58, 63–81.
Pidgeon, R.T., Nemchin, A.A., Hitchen, G.J., 1998. Internal structures of zircons from Archaean granites from the Darling Range batholith: implications for zircon stability and the interpretation of zircon U–Pb ages. Contributions to Mineralogy and Petrology 132, 288–299.
Pidgeon, R.T., Macabira, M.J.B., Lafon, J.M., 2000. Th–U–Pb isotopic system and internal structures of complex zircon from an enderbite from the Pium Complex, Caraja's Province, Brazil: evidence for the ages of granulite facies metamorphism and the protolith of the enderbite. Chemical Geology 166, 159–171.
Poujol, M., Kiefer, R., Robb, L.J., Anhaeusser, C.R., Armstrong, R.A., 2005. New U–Pb data on zircons from the Amalia greenstone belt, Southern Africa: insights into the Neoarchaean evolution of the Kaapvaal Craton. South African Journal of Geology 108, 317–332.
Rosa-Costa, L.T., Lafon, J.M., Delor, C., 2006. Zircon geochronology and Sm–Nd isotopic study: further constraints for the Archean and Paleoproterozoic geodynamical evolution of the southeastern Guiana Shield, north of Amazonian Craton, Brazil. Gondwana Research 10, 277–300.
Rosa-Costa, L.T., Lafon, J.M., Cocherie, A., Delor, C., 2008. Electron microprobe U–Th–Pb monazite dating of the Transamazonian high-grade metamorphic overprint on Archean rocks from Amapá Block, southeastern Guiana Shield, northern Brazil. Journal of South American Earth Sciences 26, 445–462.
Rudnick, R.L., Gao, S., 2005. Composition of the continental crust. In: Rudnick, R.L. (Ed.), The Crust. Treatise on Geochemistry, vol. 3. Elsevier-Pergamon, Oxford, pp. 1–64.
Sapienza, G.T., Griffin, W.L., O'Reilly, S.Y., Morten, L., 2007. Crustal zircons and mantle sulfides: Archean to Triassic events in the lithosphere beneath south-eastern Sicily. Lithos 96, 503–523.
Santos, J.O.S., Hartmann, L.A., Bossi, J., Campal, N., Schipilov, A., Piñeyro, D., McNaughton, N.J., 2003. Duration of the Trans-Amazonian cycle and its correlation within South America based on U–Pb SHRIMP geochronology of the La Plata Craton, Uruguay. International Geology Review 45, 27–48.
Santos, T.J.S., Fetter, A.H., Van Schmus, W.R., Hackspacher, P.C., 2009. Evidence for 2.35 to 2.30 Ga juvenile crustal growth in the northwest Borborema Province, NE, Brazil. In: Reddy, S.M., Mazumder, R., Evans, D.A.D., Collins, A.S. (Eds.), Palaeoproterozoic Supercontinents and Global Evolution. Geological Society, London, Special Publications 323, 271–281.
Sylvester, P.J., 1998. Post-collisional strongly peraluminous granites. Lithos 45, 29–44.
Taylor, S.R., McLennan, S.M., 1985. The Continental Crust: Its Composition and Evolution. Blackwell Scientific Publications, Oxford, pp. 1–312.
Teixeira, K.S.L., Moura, C.A.V., Truckenbrodt, W., Klein, E.L., Chemale Jr., F., 2007. Petrografia, geoquímica e geocronologia da Formação Igarapé de Areia,

NE – Pará. In: Congresso Brasileiro de Geoquímica, 11, Atibaia, São Paulo, Anais, (CD-ROM).
Thompson, R.N., 1982. British Tertiary province. Scottish Journal of Geology 18, 49–107.
Torquato, J.R., Cordani, U.G., 1981. Brazil–Africa geological links. Earth-Science Reviews 17, 155–176.
Vasquez, M.L., Macambira, M.J.B., Armstrong, R.A., 2008. Zircon geochronology of granitoids from the western Bacajá domain, southeastern Amazonian craton, Brazil: Neoarchean to Orosirian evolution. Precambrian Research 161, 279–302.
Vavra, G., Schmid, R., Gebauer, D., 1999. Internal morphology, habit and U–Th–Pb microanalysis of amphibole to granulite facies zircon: geochronology of the Ivren Zone (Southern Alps). Contributions to Mineralogy and Petrology 134, 380–404.
Villaros, A., Stevens, G., Moyen, J.F., Buick, I.S., 2009. The trace element compositions of S-type granites: evidence for disequilibrium melting and accessory phase entrainment in the source. Contributions to Mineralogy and Petrology 158, 543–561.
Villas, R.N.N., Sousa, F.D.S., 2007. O granito de duas micas Ney Peixoto, nordeste do Pará: aspectos petrológicos e significado tectônico. Revista Brasileira de Geociências 37, 3–16.
Whalen, J.B., Currie, K.L., Chappell, B.W., 1987. A-type granites: geochemical characteristics, discrimination and petrogenesis. Contributions to Mineralogy and Petrology 95, 407–419.
Williams, I.S., Claesson, S., 1987. Isotopic evidence for the Precambrian Province and Caledonian metamorphism of high grade paragneisses from the Seve Nappes. Scandanavian Caledonides: Contributions to Mineralogy and Petrology 97, 205–217.
Wu, Y., Zheng, Y., 2004. Genesis of zircon and its constraints on interpretation of U–Pb age. Chinese Science Bulletin 49, 1554–1569.
Zinger, T.F., Levchenkov, O.A., 2003. Comparison of the morphology, U–Pb age and Th/U ratio of zircons from a migmatite and its protolith from the central part of the Belomorian mobile belt, Russia. Geophysical Research Abstracts 5, 01033.